Origin of dust size variability in central East Antarctica (Dome B): atmospheric transport from expanded South American sources during Marine Isotope Stage 2.

Barbara Delmonte(*)[1], Chiara Ileana Paleari[1], Sergio Andò[1], Eduardo Garzanti[1], Per Sune Andersson[2], Jean Robert Petit[3], Xavier Crosta[4], Biancamaria Narcisi[5], Carlo Baroni[6], Maria Cristina Salvatore[6], Giovanni Baccolo[1], Valter Maggi[1].

(*) corresponding author. *barbara.delmonte@unimib.it*

1-Department of Earth and Environmental Sciences (DISAT), University Milano-Bicocca, Piazza della Scienza, 20126 Milano, Italy

2-Department of Geosciences, Swedish Museum of Natural History, Box 50 007, SE-104 05 Stockholm, Sweden

3-Univ. Grenoble Alpes, CNRS, IRD, IGE, F-38000 Grenoble, France

4-UMR-CRS 5805 EPOC, Université de Bordeaux, Avenue Geoffroy Saint Hilaire CS50023, 33615 Pessac Cedex, France

5-ENEA, C.R. Casaccia, 00123 Roma, Italy

6-Dipartimento di Scienze Della Terra, University of Pisa, Via S. Maria N. 53, 56126, Pisa, Italy

ABSTRACT

We here investigate the spatial and temporal variability of eolian dust particle sorting recorded in Dome B (77° 05' S, 94° 55' E) ice core, central East Antarctica, during Marine Isotope Stage (MIS) 2. We address the question whether such changes reflect variable transport pathways from a unique source area or rather a variable apportionment from diverse Southern Hemisphere sources transported at different elevation in the troposphere. The Sr-Nd radiogenic isotope composition of glacial dust samples as well as single-particle Raman mineralogy support the hypothesis of a unique dust provenance both for coarse and fine mode dust events at Dome B. The southern South American provenance of glacial dust in Antarctica deduced from these results indicate a dust composition coherent with a mixture of volcanic material and minerals derived from metamorphic and plutonic rocks. Additionally, Dome B glacial samples contain aragonite particles along with diatom valves of marine benthic/epiphytic species and freshwater species living today in the northern Antarctic Peninsula and southern South America. These data suggest contribution from the exposed Patagonian continental shelf and glacial outwash plains of southern Patagonia at the time when sea level reached its minimum. Our results confirm that dust sorting is controlled by the relative intensity of the two main patterns of tropospheric dust transport onto the inner Plateau, i.e. fast low-level advection and long-range high-altitude transport including air subsidence over Antarctica.

KEYWORDS

Quaternary; Paleoclimatology; Antarctica; ice cores; dust; provenance; Marine Isotope Stage 2; micron-size particle Raman mineralogy

HIGHLIGHTS

► South American provenance of coarse- and fine-mode dust events at Dome B (Antarctica)

► Atmospheric circulation controls dust size variability in Antarctic ice cores

► The Patagonian shelf became an important dust source during MIS 2 sea level minimum

► Importance of Southern Patagonian glacial dust sources

► Raman determination of micron-size mineral grains

INTRODUCTION

Ice cores provide direct and highly-resolved records of climate and aerosol load of the atmosphere over different timescales (EPICA Community Members, 2004; Kawamura et al., 2017; Petit et al., 1999). They record atmospheric parameters as well as forcing factors of global significance such as greenhouse gases, and of more regional significance such as mineral dust aerosol. The eolian dust record from EPICA Dome C (Lambert et al., 2008) along with the paleo-temperature record inferred from stable isotopes of water (Jouzel et al., 2007) allowed assessing climate and atmospheric circulation changes in the Southern Hemisphere over the past ~800 kyrs. By showing a significant correlation between dust flux and temperature during cold glacial periods, which is absent during interglacial periods, the EPICA Dome C dust record provided robust evidence for a progressive coupling of Antarctic and southern Hemisphere climate as temperature became colder (Lambert et al., 2008).

The first-order covariance among ice core dust records from different parts of East Antarctica (Petit & Delmonte, 2009) suggests a broad uniformity in the dust input onto the Plateau. During MIS 2 (~19-30 kyr BP), the last glacial period, the general uniformity of glacial dust flux contrasts with the regionally-variable character of eolian mineral dust size (Delmonte et al., 2004a), a parameter linked to transport processes. Such differences were interpreted as the expression of different atmospheric pathways for dust windborne to the polar area (Delmonte et al., 2004a).

Eolian dust reaching central East Antarctica is micron-sized and well-sorted, as a consequence of long-distance atmospheric transport (Petit & Delmonte, 2009). The spherical-equivalent diameter of background dust particles is smaller than 5 µm and the modal value of dust mass-size distribution is generally around 2 µm. A previous study on the Dome B ice core (Delmonte et al., 2004a), drilled in the Antarctic interior (figure 1), revealed clear oscillations in the modal diameter of particles (spanning from 2.0 to 2.7 µm) during MIS 2 and a subsequent decrease throughout the last termination until the Holocene, when particles became smaller (~1.8 µm). This glacial/interglacial pattern of changes observed at Dome B is opposite to what is observed in other areas of the Antarctic Plateau such as Dome C and Komsomolskaya (figure 1). Superimposed on glacial/interglacial trends, dust size oscillations occur over a wide range of periodicities (Delmonte et al., 2004a; 2005; Wegner et al., 2015). The underlying mechanism proposed for the interpretation of dust grading in central East Antarctic ice cores associates small particles to long-range high-altitude transport including mass convergence in the middle troposphere above Antarctica and subsequent air subsidence. Conversely, large particles are associated to lower-level advection events linked to the presence of cyclonic systems off the Antarctic coast including short-cut advections from the South Atlantic Ocean (Krinner and Genthon, 2003; Krinner et al., 2010). Interestingly, model-based investigations show that both during the Last Glacial Maximum (LGM) and today South American dust is transported over Antarctica at lower levels with respect to Australian dust (Albani et al., 2012; Krinner et al., 2010; Li et al., 2008).

Previous studies based on Sr and Nd radiogenic isotopes on several East Antarctic ice core sections, integrated to obtain a few large samples, concluded that southern South America was the major dust supplier for central East Antarctica during MIS 2 (Basile et al., 1997; Delmonte et al., 2004a, 2004b; Grousset et al., 1992), as supported by Pb isotope data (Vallelonga et al., 2010) and Rare Earth Elements patterns (Gabrielli et al., 2010). According to these studies, source regions include Patagonia and possibly the Pampas region and generally the southern part of Central Western Argentina at lower latitude (Basile et al., 1997; Gaiero et al., 2007; Gaiero 2007; Gili et al. 2016 and in review). During glacial-climate conditions, the so called *source intensity changes* in South America include: (I) increased dust production and deflation resulting from enhanced aridity and reduced continental vegetation (Basile et al., 1997; Mahowald et al., 1999); (II) intensified surface wind intensities (Werner et al., 2002) and foehn winds on the lee side of the Andes resulting from the increased volume of the Patagonian ice sheet (Kaiser and Lamy, 2010 and references therein); (III) increased amount of fine sediments resulting from rock-flour production and deposition on the Patagonian glacial outwash plains (Sugden et al., 2009); and finally, (IV) expansion of deflation areas following exposure of the expanded Argentine/Patagonian continental shelf during glacio-eustatic low stand (Grousset et al., 1992). The 120-130 m sea-level drop during the last glacial (Spratt & Lisiecki, 2016 and references therein) approximately doubled the modern continental surface available for deflation around southern South America (figure 1). This source expansion contributed to the exacerbation of the continental character of climate both in the Pampas and in Patagonia. The role of the Patagonian continental shelf as dust source to Antarctica during MIS 2 is however still controversial (Basile et al., 1997; Gaiero et al., 2003; 2007; Kaiser and Lamy, 2010). Dust entrained from the shelf displays a geochemical signature similar to sedimentary and volcanic detritus produced in the adjacent continent (Gaiero et al., 2003; De Mahiques et al., 2008). Moreover, the sharp dust decrease at the end of the last glacial period was not in phase with sea level rise (Wolff et al., 2006) (figure 2A). Whether the areal expansion of the South American source actually translated into more dust transported to East Antarctica remains as an open question.

In this work we address the issue raised originally by Krinner et al. (2010) whether dust particle size variability recorded in Antarctic ice cores may reflect atmospheric transport from a single source area exclusively or a variable dust apportionment from different sources (e.g., Australia and South America), modulated in turn by source intensity changes and/or atmospheric transport. We tackled this issue by analyzing the Sr and Nd isotopic composition of well-selected *coarse-mode* and *fine-mode* dust events from the glacial (MIS 2) and early deglacial portion of Dome B ice core (figure 1). The strontium and neodymium radiogenic isotope fingerprint of dust, commonly used in Antarctic ice core research to discriminate among dust sources (Grousset and Biscaye, 2005), is here complemented by single-grain Raman mineralogical analyses performed on a subset of dust samples. This innovative technique allows us to identify all mineral species and polymorphs constituting the sample, along with their relative abundances (Andò et al., 2011; Andò & Garzanti, 2014), providing crucial information to draw conclusions about parent rocks and conditions under which the sediment formed (Godoi et al., 2006; Villanueva et al., 2008). By coupling these two powerful complementary approaches with microscopic observations we could assess robustly the origin of glacial dust size changes recorded in the Antarctic ice cores, provide further evidence for South American provenance of dust deposited in inner Antarctica during MIS 2, and clarify the role of the Patagonian continental shelf and continental southernmost regions as dust source at times of minimum sea level reached during MIS 2.

1. METHODS

Dome B is a high-elevation site (3650 m a.s.l.) located in central East Antarctica about 850 km from where the *old* Dome C ice core (Lorius et al., 1979) was drilled. At Dome B, a 780 m-deep ice core was drilled during austral summer 1987-1988 in the framework of the 33rd Soviet Antarctic expedition. The climatic record from Dome B covers the last 30 kyr (figure 2A) and was documented by Jouzel et al. (1995) along with a first chronology and a pilot dust-concentration profile, defined later in detail (figure 2B) by Delmonte et al. (2004a). The choice of this ice core for our purpose is motivated by clearer evidence of pronounced dust size changes than in other ice cores of the East Antarctic Plateau. This study benefited from the more recent AICC2012 chronology (Veres et al., 2013), that was fitted on the stable isotope (δD) record from Dome B (Jouzel et al., 1995).

2.1 *Dust concentration and grain-size*

At EuroCold Laboratory of DISAT (University Milano-Bicocca), a set of 10 ice-core *bags* (i.e. entire ice-core pieces, 60 to 90 cm-long each) from Dome B was selected between 520 and 700 m depth. Ice cores were sub-sampled at ~3 cm resolution. The age of these samples spans from ~16.5 to ~28.5 kyr BP, corresponding to the Last Glacial Maximum and the very first part of the last climatic transition (figure 2A, 2B). We adopted the same procedure for sampling three additional ice-core bags from the older (glacial) part of the *old* Dome C ice core (Lorius et al., 1979), spanning from ~20.4 kyr BP to ~22.8 kyr BP. Dust concentration and grain-size distribution were measured on each subsample in clean room (ISO6), following the same analytical protocol adopted in Delmonte et al., (2004a). In this work, we used a Beckman Coulter Multisizer™ 4e COULTER COUNTER® set to measure particles with equivalent spherical diameter between 0.6 and 18 µm. Data treatment include calculation of particle-size indicators including the Fine Particle Percentage (FPP, %) defined as the percentage of mass represented by particles having equivalent spherical diameter between 1 and 2 µm over the total mass of sample, conventionally included between 0.7 and 5 µm (Delmonte et al., 2004a, 2005). The mode of the volume (mass) size distribution was estimated by fitting the particle volume-size distributions with a four-parameter Weibull function described in Delmonte et al. (2002). Results for Dome B are shown in figures 2B and 2C along with earlier data from the same core (Delmonte et al., 2004a).

Optical-microscope observations were performed on most Dome B samples analysed by Coulter Counter (figure 2B), whereas Scanning Electron Microscope (SEM) pictures were taken on a selected number of specimens.

2.2 Sr and Nd-isotope signatures

A set of 9 samples displaying different dust mode (from ~2 µm to 2.7 µm) and concentration (from 450 to 1900 ppb) were selected from the Dome B ice core along with three samples from the *old* Dome C ice core. Information about age, concentration and grain size of dust samples is provided in table 1. Before sample selection for isotope geochemistry, careful inspection of particle-size spectra was done to avoid unintentional sampling of ice sections containing cryptotephra layers, which can be generally distinguished from *background* dust samples (Narcisi et al., 2012). Dust extraction was performed in clean room (ISO6) following the protocol developed by Delmonte et al. (2008). At the Department of Geosciences at the Swedish Museum of Natural History in Stockholm, dust samples (about 100 µg each) were digested in an acid mixture (HNO_3+HF+$HClO_4$) and heated (~60°C) in closed vessels for 24h. After isotopic enrichment (^{147}Sm/^{150}Nd and ^{84}Sr enriched spikes) the solution was evaporated to dryness on a hot plate. The residue was dissolved in 4 ml 6M HCl and subjected to the chemical procedures for elemental separation described in Delmonte et al. (2008, supplementary online material).

Samples were analysed on a Thermo Scientific TRITON TIMS (Thermal Ionization Mass Spectrometer). Neodymium was loaded mixed with Alfa Aesar graphite on double rhenium filaments and run as metal in static mode using rotating gain compensation. Ratios were reduced assuming exponential fractionation. Calculated ratios were normalised to ^{146}Nd/^{144}Nd = 0.7219. The external precision for ^{143}Nd/^{144}Nd as judged from running small (2 ng) loads of nNdβ standard was 0.511910±0.000038 (2 std.dev., n=10). No accuracy correction was applied because the ^{143}Nd/^{144}Nd ratio for the nNdβ standard was 0.511910. The epsilon units are calculated as follows:

$\varepsilon_{Nd}(0) = [(^{143}Nd/^{144}Nd)_{sample}/(^{143}Nd/^{144}Nd)_{CHUR}-1] \times 10^4$; (with $^{143}Nd/^{144}Nd_{CHUR}$ =0.512638).

The purified Sr samples were mixed with tantalum activator and loaded on a single rhenium filament. Two hundred 8 s integrations were recorded in multi-collector static mode, applying rotating gain compensation. Measured ^{87}Sr intensities were corrected for Rb interference using ^{87}Rb/^{85}Rb = 0.38600 and ratios were reduced using the exponential fractionation law and ^{88}Sr/^{86}Sr = 8.375209. The external precision for ^{87}Sr/^{86}Sr as judged from running small (2 ng) 987 standard was 0.710213±0.000028 (2 std. dev., n=10). An accuracy correction was applied, because the ^{87}Sr/^{86}Sr ratio measured for the NBS 987 standard was 0.710213, deviating from the generally accepted value of 0.710245. The results are reported in table 1.

2.3 Micron-size-particle Raman mineralogy

Single-grain mineralogical investigations by Raman spectroscopy were performed on a subset of four samples selected from the Dome B ice core between ~21.7 and 24.7 kyrs BP, thus very close to the MIS 2 sea-level minimum. The samples selected displayed different dust size distribution and concentration. Given the very small size of particles (∅ <5 µm), we developed first a dedicated protocol for extraction, preparation and analysis of ice-core dust samples to guarantee the best analytical conditions (Paleari et al., in preparation).

Measurements were recorded on an InVia Renishaw micro-Raman spectrometer (Nd YAG laser source, λ=532 nm) installed at the *Laboratory for Provenance Studies* of DISAT (University Milano-Bicocca). For each dust grain, a minimum of four consecutive acquisitions was acquired. A total of 632 spectra were obtained for the four investigated samples (~160 particles per sample on average), excluding particles giving no signal (e.g. volcanic glasses), containing carbon possibly because contamination during laboratory work, and particles with undetermined spectra. Results are reported in table 2.

RESULTS AND DISCUSSION

3.1 GLACIAL DUST CONCENTRATION AND SIZE VARIABILITY AT DOME B

Dust concentration at Dome B during MIS 2 is calculated as 780±380 ppb by averaging bag-mean values. Such concentration is ~50 higher than during Holocene times (figure 2B), in agreement with previous findings (Delmonte et al., 2004a). A similar huge increase in dust concentration by a factor of ~50 during the MIS 2 was documented in EDC (Lambert et al., 2008) and EPICA Dronning Maud Land (EDML) ice cores (Wegner et al., 2015). At Dome B, dust-volume (mass) size distribution shows modal values oscillating between ~2 µm and ~2.7 µm (figure 3A, 3B), ~2.4 µm on average (table 1). This corresponds to FPP values between 50% and 30% (figure 3C). As observed in Delmonte et al. (2004a), dust particles windborne to Dome B during the last glacial period are larger than those deposited at Dome C. Data from the EPICA-Dome C (Delmonte et al., 2004a) and the *old* Dome C (table 1) show modal values of particle-size distribution around 1.9-2.0 µm during MIS 2 and FPP values of 48±3%.

Detailed dust size measurements carried out for each bag (each representing ~50-60 years) highlight a clear high-frequency (decadal) mode of variability at Dome B (figure 2C). Within a single bag, FPP variations (Δ ~28%) are comparable to secular and millennial-scale dust size cycles detected from low-resolution records. This is not the case for the *old* Dome C, where FPP variability within each bag is lower (Δ < 10%). Such pronounced dust size variability at Dome B denotes a more variable character of glacial dust transport to this site with respect to other parts of the plateau like Dome C. High-resolution measurements are thus essential when investigating dust size changes in this part of Antarctica during the last glacial period.

A positive correlation (r = ~0.67) between glacial dust concentration and grain size is observed at Dome B when concentration exceeds ~300 ppb (figure 3C). Large dust particles are associated with high dust concentrations in ice, and vice versa. The same relationship was observed in the older (glacial) part of the EDML ice core (Wegner et al., 2015) and ascribed to the varying intensity of glacial dust transport.

3.2 ISOTOPIC CONSTRAINTS ON GLACIAL DUST PROVENANCE

The Sr and Nd isotope ratios of MIS 2 dust at Dome B and Dome C (figures 4, 5A and 5B) are tightly clustered ($-3.1 < \varepsilon_{Nd}(0) < -0.5$; $0.7083 < {}^{87}Sr/{}^{86}Sr < 0.7098$), plotting within the isotopic field previously defined for MIS 2 dust in central

East Antarctica (Basile et al., 1997; Delmonte et al., 2004a, 2004b). Dome B isotopic data are reported in figure 4. The lack of correlation of isotopic composition with particle size (and thus also with dust concentration; figure 3C) suggests that *coarse mode* and *fine mode* dust events are geochemically similar and thus originated in the same source area, as also indicated by the mineralogical composition of samples (see below). Independently of dust grain size, Antarctic ice core data for MIS 2 appear aligned along a hypothetical mixing hyperbola from $\varepsilon_{Nd}(0)$ ~-0.5 and $^{87}Sr/^{86}Sr$~ 0.7083 to $\varepsilon_{Nd}(0)$ ~-3 and $^{87}Sr/^{86}Sr$~ 0.7098, a small interval indeed for both variables. The only outlier is represented by the very first isotopic ratio for the *old* Dome C core reported by Grousset et al. (1992), indicated in figure 4, which might be explained by the presence of invisible cryptotephra layer(s) within the large part of core (from 550 to 590 m) sampled in that pioneering study. We do not consider this sample as representative of background dust, also because sample ODC588 (table 1, figure 4) selected in the present work from the same core at similar depth falls within the isotopic field of the rest of samples.

Isotopic data of glacial dust from Dome B and other central East Antarctic ice cores are compared in figure 5A to the fine fraction (∅ <5 µm or ∅ <10 µm, depending on samples) of samples selected from the two major potential dust sources in the southern Hemisphere, South America and Australia. Most likely source areas in Australia are located mainly in the eastern and south-eastern part of the continent, whereas Western Australia deserts are generally not considered to be important atmospheric sources for dust transported long range (Gingele & DeDeckker, 2005; Revel-Rolland et al., 2006). The isotopic field for fine-grained Australian dust and river clays is very dispersed, and characterised by $^{87}Sr/^{86}Sr$ ratio higher than ~0.709 and by $\varepsilon_{Nd}(0)$ between +1 and −15. Taking $\varepsilon_{Nd}(0)$ into account, only few of the Australian sediment samples (Darling river basin clays and one sample from Lake Eyre) overlap with the Nd isotopic composition of Antarctic glacial dust. Those Australian samples are very rich in kaolinite and smectite (Gingele & De Deckker, 2005; Revel-Rolland et al., 2006), which are lacking in Antarctic ice-core dust (see below). We thus discard the possibility of significant Australian contribution to the glacial dust input in Antarctica.

The isotopic field of South American dust and fine-grained sediments, including eolian dust, loess, topsoils, alluvial fans and salar edges, sediments from glacial outwash plains, Patagonian rivers, and the Argentine continental shelf (Basile et al., 1997; Delmonte et al., 2004b; Gaiero et al., 2003; Gaiero et al., 2007; Gaiero 2007; Gili et al., in review; Sugden et al., 2009) is more restricted than that of Australian samples and is consistent with the Antarctic dust field (figure 5B). The Nd isotope interval indicated for sediments of the Argentine continental shelf south of the Rio de la Plata estuary is $-4 < \varepsilon_{Nd}(0) < -0.1$ (De Mahiques et al., 2008; highlighted in yellow in figure 5B). Shelfal samples have similar $\varepsilon_{Nd}(0)$ values as Patagonian river sediments and, in general, as dust and sediment samples from the nearby continent, as expected from the Andean origin of shelf sediments (e.g. De Mahiques et al., 2008; Gaiero et al., 2003). According to Gaiero et al. (2003), both during the last glacial period and today the largest part of the sediment mass derived from the Andes and transported across Patagonia to the shelf by rivers has been ultimately supplied to the shelf by eolian action, which explains the homogenized geochemical signature. The $\varepsilon_{Nd}(0)$ values of dust from Antarctic ice cores match those of samples derived from Patagonia, and specifically from Tierra del Fuego, including the continental shelf. The slight Sr isotopic difference between some source samples and glacial dust may be ascribed to Sr isotopic fractionation by particle size (e.g. Gaiero et al., 2007) or to the presence of carbonates, as discussed below.

3.3 MINERALOGICAL EVIDENCE

Single-grain Raman spectroscopy analysis was performed on four samples from Dome B displaying variable mode (2 µm to 2.7 µm) and concentration in ice (600 ppb to >1400 ppb). The relative abundance of the identified mineral species, including quartz and other SiO_2 polymorphs, feldspars, phyllosilicates, carbonates, pyroxene and other heavy minerals, Fe-oxides and hydroxides, Ti-oxides, Al-hydroxides and zeolites, is expressed as frequency of counted grains in table 2. These minerals have different origin (figure 6), including: (1) terrigenous grains eroded from rock assemblages of the continental crust; (2) grains derived from penecontemporaneous volcanic sources; and (3) grains of marine origin (e.g., aragonite). Terrigenous minerals (quartz, feldspars, muscovite) represent 70-84% of the dust. Calcite also occurs. Volcanic-derived minerals (sanidine, zeolites) represent 5-15% of the dust, but this range does not include volcanic glass - commonly observed under the microscope but hardly distinguished by Raman analysis - and thus notably underestimates volcanic contribution. Kaolinite and smectite have not been found; this is coherent with previous studies on glacial ice from Vostok and Dome C (Gaudichet et al., 1986; 1988), where these minerals were extremely rare or absent. Because these clay minerals are instead abundant in Australian soils and river sediments, a very limited role of Australian dust sources under glacial conditions is indicated. Iron oxides and hydroxides are largely derived from soils. Samples DB620, DB631 and DB640 include common aragonite (representing 21% of sample DB631; table 2, figure 6), a mineral reported here for the first time in Antarctic ice cores. Aragonite, a polymorph known to form under a much narrower range of conditions than calcite, represents an important component of the total particulate calcium carbonate in the oceans. It is mainly biogenic, but may form also by inorganic processes in marine or freshwater environments (Folk, 1974). Aragonite thus assumes a special significance for our goals, as it can be considered as indicative of provenance from shallow sea-floors. The presence of carbonates and especially of aragonite also involves important questions about the interpretation of $^{87}Sr/^{86}Sr$ ratios obtained from unleached ice-core dust samples, because Sr is a main substituent for Ca in the carbonate lattice and therefore aragonite and calcite represent a major sink for dissolved Sr in ocean water. The Sr isotopic ratio obtained from our dust samples including significant calcium carbonate formed in the ocean is therefore biased towards the seawater ratio ($^{87}Sr/^{86}Sr$ =0.7092; McArthur, 2010).

Differently from the other three samples, sample DB600 is dominated by terrigenous minerals, with subordinate volcanic minerals, very rare aragonite and apparent lack of calcite. No evident relationship between mineralogy and grain size has been observed in any of the samples.

3.4 PALEONTOLOGICAL EVIDENCE

The occurrence of wind-reworked fossils in our dust samples represent a fundamental piece of evidence for our paleogeographic reconstruction. Samples older than ~23 kyr BP (deeper than ~620 m, yellow vertical band in figure 2) contain complete diatom valves not observed in younger samples. Diatoms, found in both fine- and coarse-grained dust indicating no association with dust concentration or size, are particularly abundant in three ice-core sections dating back to ~24 kyr BP, 26.2 kyr BP, and 28.4 kyr BP (samples DB631, DB660 and DB700). Some specimens are marine to brackish benthic/epiphytic species (figure 7A, *Diploneis* sp.) living in coastal environments of both the northern Antarctic Peninsula (Al-Handal & Wulff, 2008) and southern South America (Ferrario and Sar, 1985). But most are freshwater diatoms (*Luticola* cf *cohnii*, *Halamphora* sp.: figure 7A; *Placoneis australis*, *Planothidium* cf *rostrolanceolatum*, *Navicula* cf *shackletoni*, *Navicula cremeri*, *Navicula* cf *australohetlandica*: figure 7B) living today in habitats such as streams, lakes and their outflows, ponds and occasionally wet soil and mosses in maritime islands of the northernmost Antarctic Peninsula including the South Shetland and South Georgia Islands (Zidarova et al., 2009; Van de Vijver et al., 2011; 2012; 2013; 2014). We could not ascertain whether they also thrive in southern South America, where they might have been misidentified with similar species.

Freshwater diatoms have long been reported from the *old* Dome C ice core (Burckle et al., 1988; Ram et al., 1988), with peak occurrence during the Last Glacial Maximum and only very sporadic presence during the Holocene. Most diatom valves in Dome B glacial samples are entire and very well-preserved, thus very different from the small fragments reworked locally from Antarctic sediments as observed at Talos Dome (Delmonte et al., 2013). Specimens found at Dome B are also mainly freshwater diatoms, whereas Pliocene marine species predominate in Sirius group tillites (Scherer et al., 2016).

Diatom valves of both marine and freshwater origin are light and often aerodynamic, and can thus be lifted and transported over great distances by wind. Although the Southern Ocean may appear as a most likely source for any diatoms found in ice or till on the Antarctic continent, according to Burckle et al. (1988) and Sherer et al. (2016) surface winds over the ocean are not efficient enough to transport living diatoms at great distance from the coast, and therefore diatom valves and microclasts reaching the interior of the East Antarctic ice sheet most likely derive from fossil sources or seasonally aerophilic environments, i.e. subaerially exposed dry source beds covered with abundant unconsolidated diatoms.

3.5 GLACIAL-DUST TRANSPORT PATTERNS

Southern South America and Eastern Australia represented the two major dust sources in the Southern Hemisphere since the last glacial period (Gingele & De Deckker, 2005; Prospero et al., 2002; Revel-Rolland et al., 2006). Dust emissions from both sources increased during MIS 2, although in different proportions (e.g. Albani et al., 2012). It has been established that the fine component of dust from these sources can travel long-range to the high southern latitudes of Antarctica, although the preferential altitude of transport is different (Li et al., 2008; Krinner et al., 2010; Albani et al., 2012). Independently from climate conditions, Australian dust is transported consistently at higher elevation than dust from South America. South America has been shown to be the dominant dust source for Antarctica during MIS 2 (e.g. Basile et al., 1997; Delmonte et al., 2004a, 2004b, Gabrielli et al., 2010). Therefore, dust grading in ice cores has been related to atmospheric pathways from South America to Antarctica (Delmonte et al., 2004a; Wegner et al., 2015). Alternative explanations include differences in the relative contributions from two distinct source areas, South America and Australia, controlled by either atmospheric transport variability at different timescale or by changes in dust primary production within the source regions.

In this work, we studied individual coarse-mode and fine-mode dust events along the core, and observed among samples a homogeneous mineralogical composition and isotopic ratios. This argues against a differential apportionment from the geologically-different Australia and South America continents, which should lead to size-related geochemical and mineralogical differences. Our results suggest a unique geographic source for all glacial dust events, independently of particle grading. Dust size changes recorded in central Antarctic ice cores are thus related exclusively to the type of tropospheric transport towards the interior of the Antarctic continent. Coarse dust events are related to dust-carrying air masses with shorter and relatively low-level trajectories in the mid-troposphere, i.e. dust advections through cyclonic systems off the Antarctic coast, while fine dust events are instead related to longer circumpolar atmospheric pathways implying mass convergence in the middle troposphere and subsidence over the Antarctic Plateau. These are actually the two main typologies of tropospheric dust transport to the interior of Antarctica (Parish and Bromwich, 1991; James, 1989), whose relative intensity certainly varies in time and space. Our high-resolution analysis of Dome B ice core bags demonstrates that the relative intensity of one typology of transport over the other is expressed not only at centennial to millennial timescale as previously documented (Delmonte et al., 2004a) but also at decadal to multi-decadal timescale. The correlation between dust concentration and size at Dome B additionally suggests that dust transport from the lower atmospheric levels are also capable to bring larger amounts of dust compared to upper troposphere advections. This probably reflects different transport intensities, but whether this is related to air-mass velocity, to turbulence within the boundary layer, or to other factors such as seasonality of dust emissions and transport (Wegner et al., 2015) remains unclear. Further investigation through atmospheric circulation models that include dust-cycle dynamics are needed.

Our hypothesis about the dust size oscillations observed at Dome B can be applied not only to interpret decadal and multi-decadal variability at the site, but also to understand the reason why dust was coarser at Dome B with respect to Dome C on average during the MIS 2 (Delmonte et al., 2004a). Previous interpretations have explained the difference in dust sizes observed at the two sites in terms of different atmospheric transport altitude (Delmonte et al., 2004a). Our new results suggest that the spatial differences of dust grading onto the Plateau during MIS 2 reflect the strength and localization of tropospheric air subsidence over Antarctica, which is related to local and regional dynamics. Modelized radon-like tracer transport times from Australia and Patagonia to Antarctica during MIS 2 (Krinner and Genthon 2003; Krinner et al., 2010) show that the frequency of fast, low-level atmospheric transport was quite uniformly favored over the entire continent, possibly as a consequence of increased baroclinicity indicated by the steeper meridional temperature gradients. This is in line with evidence from Dome B, but contradicts the opposite observations reported for Dome C and other parts of the Antarctic plateau. Glacial dust model simulations from Albani et al. (2012) show an overall increase in the proportion of fine particles (<2.5 micron) in the atmosphere above Antarctica, but were unable to reproduce the opposite regional changes on the plateau because of the rough dust size resolution of the model. Further model-based investigations at high spatial and size spectral resolution are needed for Antarctica.

We are aware that dust particle size in Antarctic ice cores can be influenced also by wet or dry deposition regime, a process not taken into account in this study. The reason is that on the East Antarctic Plateau dry deposition is probably the principal way of dust deposition (Legrand and Mayewski, 1997; Wolff et al., 2006), especially for inner sites such as Dome B and Dome C where accumulation is extremely slow. It is therefore unlikely that the two sites, having similar snow accumulation rate, could be influenced by different depositional regimes, and that the high-frequency changes in dust size at Dome B could reflect rapid switches in the intensity of dry/wet deposition processes.

3.6 THE SOUTH AMERICAN DUST SOURCE DURING MIS 2

The Sr and Nd isotope fingerprint of glacial dust at Dome B, compared to potential source samples from South America and Australia, confirms earlier findings that the Patagonian region, including Tierra del Fuego, as well as lower- latitude areas in South America acted as major dust sources for central East Antarctica during the last glacial period. This is further supported by mineralogical data from single-grain Raman analyses, indicating that glacial dust deposited at Dome B is a mixture of basaltic/andesitic volcanic and terrigenous minerals derived from various rock units of the continental crust. Such a composition matches that of sediments from South America (Gaiero et al., 2003; 2007). Additionally, single-grain mineralogical data revealed the presence of carbonates, in particular of aragonite known to form preferentially in the marine environment (Folk, 1974), in Dome B glacial samples. Well-preserved marine benthic/epiphytic diatom frustules, identified today in bays of the northern Antarctic Peninsula (Al-Handal & Wulff, 2008) and southern South America (Ferrario and Sar, 1985), are common in samples older than ~ 23 kyr BP (figure 2, yellow band), suggesting that dust was deflated from exposed subaqueous/submarine environments during the MIS 2 sea-level low stand. This indicates in turn major contribution from the widely exposed Argentine shelf at the time of sea-level minimum, which because of its flat morphology became an important dust source since sea-level dropped below -80 m during the last glacial (Kaiser & Lamy, 2010; Wolff et al., 2006).

Provenance of dust from the Patagonian shelf during glacial lowstand is not in contradiction with the lack of phasing between global deglacial sea level rise and the dust fall recorded in Antarctic ice cores, because dust concentration in ice cores depends on different factors, including not only source-intensity changes but also particle lifetime in the atmosphere, which is very sensitive to climate through the hydrological cycle (Yung et al., 1996; Petit & Delmonte, 2009).

The presence of well-preserved entire and large valves belonging to freshwater diatom species living today around the northern tip of the Antarctic Peninsula (Ross Island, South Shetlands) and in the sub-Antarctic areas of the south Atlantic (South Georgia), and possibly present in southernmost South America as well (Van de Vijver, pers. comm), opens up some new questions. These non-marine diatoms thrive in ponds, lakes, seasonal melt pools and also moist soils and sediments. Partial or complete desiccation of such water bodies or ephemeral snow and ice patches can expose diatom-bearing sediments to wind transport. The maximum expansion of the Antarctic Ice Sheet between 30 and 23 kyr BP considerably reduced the exposed ice-free areas in the Antarctic Peninsula and coastal Antarctica (figure 1). Only South Georgia was partly ice-free during the Last Glacial Maximum (Hodgson et al., 2014), which is not geologically dissimilar to southern South America and thus yielding detritus with comparable geochemical and mineralogical signature. However, South Georgia is much smaller than exposed southern South American sources, especially when including the continental shelf. The most plausible provenance of freshwater diatoms in Dome B glacial samples is from the southern tip of South America. The northward shift of the Antarctic frontal zone during the last glacial period increased the influence of polar air on the southern tip of South America and temperatures in Tierra del Fuego were ~6-7 °C colder than today (Hulton et al., 2002; Moreno et al., 1999). Climate was also dryer south of 50 °S (Hulton et al., 2002), possibly as a consequence of the precipitation-shadow effect induced by growth of the southern Patagonian ice sheet (Kaplan et al., 2008). Moreover, frontal systems surrounding Antarctica were probably displaced northward because of the increased sea-ice extent in the South Atlantic (Gersonde et al., 2005; Allen et al., 2011). Our conclusions are thus fully consistent with previous suggestions by Sugden et al. (2009), who indicated glacial outwash sediments from southern Patagonia as temporarily important dust sources during MIS 2 and suggested that the expanded South Atlantic sea-ice cover and the Patagonian ice sheet forced intense weather systems through the Drake Strait leading to strong winds over the outwash plains of the dry Strait of Magellan area. Diatoms from high South American latitudes were found during the period of maximum extent of summer sea-ice in the Scotia Sea (30-22 kyr BP, Allen et al., 2011). At that time, summer sea-ice extended to 59°S, close to the modern average winter sea-ice limit, and thermal gradients as well as winds over the southern tip of South America were probably strong. These conditions could have promoted dust deflation from this area. Summer sea ice retreated back to 61°S by 22 kyr BP (Allen et al., 2011; Collins et al., 2013) probably inducing a reduction in wind intensity and/or a change in mean wind direction and explaining why diatom valves are not found between 22-18 kyr BP when dust fluxes were still high in Dome B.

Conclusions

Geochemical and mineralogical evidence points to a South American provenance of glacial dust at Dome B, irrespective of the degree of particle size and concentration. Grain-size variability of dust in central East Antarctica can thus be interpreted as controlled by alternating high- and low-level dust advection towards the polar plateau. Such variability is expressed at different timescales, from orbital to multi decadal. Compared to Dome C and other parts of East Antarctica, the relatively large windborne particles reaching Dome B during MIS 2 denote an enhanced lower tropospheric transport to the site. We provide new evidence pointing towards major contribution from the emerged, wide Argentine continental shelf at the time of minimum sea level during MIS 2. This is mainly based on the first identification of common aragonite grains and by presence of well-preserved freshwater diatoms, probably reworked from glacial outwash plains in southern Patagonia. These findings provide new constraints for ice core data interpretation and can lead to an improved understanding of the dust cycle during the last glacial period.

Acknowledgements

This work was supported by SYNTHESYS (Project SE-TAF-5636), a project supporting an integrated European infrastructure for natural history collections funded via the EC Research Infrastructure Activity, FP7 Programme. PNRA-MIUR provided financial support. We thank: Prof. Bart Van de Vjiver, Prof. Jan Risberg and Prof. Nora Maidana for helpful advices on diatom species , Frederic Parrenin for help with sample dating with AICC2012 timescale, Karin Wallner and Hans Schöberg for help during laboratory work at the Swedish Museum of Natural History. Scanning Electron Microscope (SEM) observations have been carried out at the Department of Earth and Environmental Sciences, Milano Bicocca University and at the Centro Interdipartimentale Grandi Strumenti (CIGS) University of Modena and Reggio Emilia.

REFERENCES

Albani, S., Mahowald, N. M., Delmonte, B., Maggi, V., & Winckler, G. (2012). Comparing modeled and observed changes in mineral dust transport and deposition to Antarctica between the Last Glacial Maximum and current climates. Climate dynamics, 38(9-10), 1731-1755.

Al-Handal, A. Y., & Wulff, A. (2008). Marine benthic diatoms from Potter Cove, King George Island, Antarctica. Botanica Marina, 51(1), 51-68.

Allen, C. S., Pike, J., & Pudsey, C. J. (2011). Last glacial–interglacial sea-ice cover in the SW Atlantic and its potential role in global deglaciation. Quaternary Science Reviews, 30(19), 2446-2458.

Amante, C. Eakins, B.W., 2009. ETOPO1 1 Arc-Minute Global Relief Model: Procedures, Data Sources and Analysis. NOAA Technical Memorandum NESDIS NGDC-24. National Geophysical Data Center, NOAA. doi:10.7289/V5C8276M [access date february 2017].

Andò , S., Vignola, P. & Garzanti, E. 2011. Raman counting: a new method to determine provenance of silt. Rendiconti Lincei, 22, 327–347.

Andò, S., Garzanti, E., 2014. Raman spectroscopy in heavy-mineral studies. Geological Society, London, Special Publications 386 (1), 395-412

Basile, I., Grousset, F. E., Revel, M., Petit, J. R., Biscaye, P. E., & Barkov, N. I. (1997). Patagonian origin of glacial dust deposited in East Antarctica (Vostok and Dome C) during glacial stages 2, 4 and 6. Earth and Planetary Science Letters, 146(3-4), 573-589.

Bentley, M.J., Ocofaigh, C., Anderson, J.B., Conway, H., Davies, B., Graham, A.G.C., Hillenbrand, C.-D., Hodgson, D.A., Jamieson, S.S.R., Larter, R.D., Mackintosh, A., Smith, J.A., Verleyen, E., Ackert, R.P., Bart, P.J., Berg, S., Brunstein, D., Canals, M., Colhoun, E.A., Crosta, X., Dickens, W.A., Domack, E., Dowdeswell, J.A., Dunbar, R., Ehrmann, W., Evans, J., Favier, V., Fink, D., Fogwill, C.J., Glasser, N.F., Gohl, K., Golledge, N.R., Goodwin, I., Gore, D.B., Greenwood, S.L., Hall, B.L., Hall, K., Hedding, D.W., Hein, A.S., Hocking, E.P., Jakobsson, M., Johnson, J.S., Jomelli, V., Jones, R.S., Klages, J.P., Kristoffersen, Y., Kuhn, G., Leventer, A., Licht, K., Lilly, K., Lindow, J., Livingstone, S.J., Massé, G., McGlone, M.S., McKay, R.M., Melles, M., Miura, H., Mulvaney, R., Nel, W., Nitsche, F.O., O'Brien, P.E., Post, A.L., Roberts, S.J., Saunders, K.M., Selkirk, P.M., Simms, A.R., Spiegel, C., Stolldorf, T.D., Sugden, D.E., van der Putten, N., van Ommen, T., Verfaillie, D., Vyverman, W., Wagner, B., White, D.A., Witus, A.E., Zwartz, D. (2014) - A community-based geological reconstruction of Antarctic Ice Sheet deglaciation since the Last Glacial Maximum Quaternary Science Reviews, 100, pp. 1-9.

Burckle, L. H., Gayley, R. I., Ram, M., & Petit, J. R. (1988). Diatoms in Antarctic ice cores: Some implications for the glacial history of Antarctica. Geology, 16(4), 326-329.

Delmonte, B., Petit, J., & Maggi, V. (2002). Glacial to Holocene implications of the new 27000-year dust record from the EPICA Dome C (East Antarctica) ice core. Climate Dynamics, 18(8), 647-660.

Delmonte, B., Petit, J. R., Andersen, K. K., Basile-Doelsch, I., Maggi, V., & Lipenkov, V. Y. (2004a). Dust size evidence for opposite regional atmospheric circulation changes over east Antarctica during the last climatic transition. Clim Dyn, 23(3-4), 427-438.

Delmonte, B., Basile-Doelsch, I., Petit, J. R., Maggi, V., Revel-Rolland, M., Michard, A., Jagoutz, E., Grousset, F. (2004b). Comparing the Epica and Vostok dust records during the last 220,000 years: stratigraphical correlation and provenance in glacial periods. Earth-Science Reviews, 66(1), 63-87.

Delmonte, B., Petit, J. R., Krinner, G., Maggi, V., Jouzel, J., & Udisti, R. (2005). Ice core evidence for secular variability and 200-year dipolar oscillations in atmospheric circulation over East Antarctica during the Holocene. Climate dynamics, 24(6), 641-654.

Delmonte, B., Andersson, P. S., Hansson, M., Schöberg, H., Petit, J. R., Basile-Doelsch, I., & Maggi, V. (2008). Eolian dust in East Antarctica (EPICA-Dome C and Vostok): Provenance during glacial ages over the last 800 kyr. Geophysical Research Letters, 35(7).

Delmonte, B., Baroni, C., Andersson, P. S., Narcisi, B., Salvatore, M. C., Petit, J. R., Scarchilli, C., Frezzotti, M., Albani, S., Maggi, V. (2013). Modern and Holocene aeolian dust variability from Talos Dome (Northern Victoria Land) to the interior of the Antarctic ice sheet. Quaternary Science Reviews, 64, 76-89.

De Mahiques, M. M., Tassinari, C. C. G., Marcolini, S., Violante, R. A., Figueira, R. C. L., da Silveira, I. C. A., Burone, L., Sousa, S. H. D. M. (2008). Nd and Pb isotope signatures on the Southeastern South American upper margin: Implications for sediment transport and source rocks. Marine Geology, 250(1), 51-63.

EPICA Community Members, 2004. Eight glacial cycles from an Antarctic ice core. Nature 429, 623–628.

Ferrario M.E. and Sar E., Consideraciones taxonomicas sobre diatomeas epifitas del intermareal rocoso marplatense. II. 1985. Revista del Museo de La Plata, Seccion Botanica, 88, 11-27.

Folk, R.L. (1974). The natural history of crystalline calcium carbonate: effect of magnesium content and salinity. Journal of Sedimentary Petrology, 44(1), 40-53.

Fretwell, P., Pritchard, H. D., Vaughan, D. G., Bamber, J. L., Barrand, N. E., Bell, R., Bianchi, C., Bingham, R. G., Blankenship, D. D., Casassa, G., Catania, G., Callens, D., Conway, H., Cook, A. J., Corr, H. F. J., Damaske, D., Damm, V., Ferraccioli, F., Forsberg, R., Fujita, S., Gim, Y., Gogineni, P., Griggs, J. A., Hindmarsh, R. C. A., Holmlund, P., Holt, J. W., Jacobel, R. W., Jenkins, A., Jokat, W., Jordan, T., King, E. C., Kohler, J., Krabill, W., Riger-Kusk, M., Langley, K. A., Leitchenkov, G., Leuschen, C., Luyendyk, B. P., Matsuoka, K., Mouginot, J., Nitsche, F. O., Nogi, Y., Nost, O. A., Popov, S. V., Rignot, E., Rippin, D. M., Rivera, A., Roberts, J., Ross, N., Siegert, M. J., Smith, A. M., Steinhage, D., Studinger, M., Sun, B., Tinto, B. K., Welch, B. C., Wilson, D., Young, D. A., Xiangbin, C., and Zirizzotti, A. (2013) - Bedmap2: improved ice bed, surface and thickness datasets for Antarctica. The Cryosphere, 7, 375-393, doi:10.5194/tc-7-375-2013.

Gabrielli, P., Wegner, A., Petit, J. R., Delmonte, B., De Deckker, P., Gaspari, V., Fischer, H., Ruth, U., Kriews, M., Boutron, C., Cescon, P., Barbante, C. (2010). A major glacial-interglacial change in eolianeolian dust composition inferred from Rare Earth Elements in Antarctic ice. Quaternary Science Reviews, 29(1), 265-273.

Gaiero, D. M., Probst, J. L., Depetris, P. J., Bidart, S. M., & Leleyter, L. (2003). Iron and other transition metals in Patagonian riverborne and windborne materials: geochemical control and transport to the southern South Atlantic Ocean. Geochimica et Cosmochimica Acta, 67(19), 3603-3623.

Gaiero, D. M., Brunet, F., Probst, J. L., & Depetris, P. J. (2007). A uniform isotopic and chemical signature of dust exported from Patagonia: Rock sources and occurrence in southern environments. Chemical Geology, 238(1), 107-120.

Gaiero, D. M. (2007). Dust provenance in Antarctic ice during glacial periods: From where in southern South America?. Geophysical Research Letters, 34(17).

Gaudichet, A., Petit, J. R., Lefevre, R., & Lorius, C. (1986). An investigation by analytical transmission electron microscopy of individual insoluble microparticles from Antarctic (Dome C) ice core samples. Tellus B, 38(3-4), 250-261.

Gaudichet, A., De Angelis, M., Lefevre, R., Petit, J. R., Korotkevitch, Y. S., & Petrov, V. N. (1988). Mineralogy of insoluble particles in the Vostok Antarctic ice core over the last climatic cycle (150 kyr). Geophysical Research Letters, 15(13), 1471-1474.

Gersonde, R., Crosta, X., Abelmann, A., & Armand, L. (2005). Sea-surface temperature and sea ice distribution of the Southern Ocean at the EPILOG Last Glacial Maximum—a circum-Antarctic view based on siliceous microfossil records. Quaternary Science Reviews, 24(7), 869-896.

Gili, S., Gaiero, D. M., Goldstein, S. L., Chemale Jr, F., Koester, E., Jweda, J., Vallelonga, P., Kaplan, M. R. (2016). Provenance of dust to Antarctica: A lead isotopic perspective. Geophysical Research Letters, 43(5), 2291-2298.

Gingele, F. X., & De Deckker, P. (2005). Clay mineral, geochemical and Sr–Nd isotopic fingerprinting of sediments in the Murray–Darling fluvial system, southeast Australia. Australian Journal of Earth Sciences, 52(6), 965-974.

Godoi, R. H. M., Potgieter-Vermaak, S., De Hoog, J., Kaegi, R. & Van Grieken, R. 2006. Substrate selection for optimum qualitative and quantitative single atmospheric particles analysis using nanomanipulation, sequential thin-window electron probe X-ray microanalysis and micro Raman spectrometry. Spectrochimica Acta, Part B, 61, 375–388.

Grousset, F. E., Biscaye, P. E., Revel, M., Petit, J. R., Pye, K., Joussaume, S., & Jouzel, J. (1992). Antarctic (Dome C) ice-core dust at 18 ky BP: Isotopic constraints on origins. Earth and Planetary Science Letters, 111(1), 175-182.

Grousset, F. E., & Biscaye, P. E. (2005). Tracing dust sources and transport patterns using Sr, Nd and Pb isotopes. Chemical Geology, 222(3), 149-167.

Hodgson, D. A., Graham, A. G., Griffiths, H. J., Roberts, S. J., Cofaigh, C. Ó., Bentley, M. J., & Evans, D. J. (2014). Glacial history of sub-Antarctic South Georgia based on the submarine geomorphology of its fjords. Quaternary Science Reviews, 89, 129-147.

Hulton, N. R., Purves, R. S., McCulloch, R. D., Sugden, D. E., & Bentley, M. J. (2002). The Last Glacial Maximum and deglaciation in southern South America. Quaternary Science Reviews, 21(1), 233-241.

James, I. N. (1989). The Antarctic drainage flow: Implications for hemispheric flow on the Southern Hemisphere. Antarctic Science, 1(03), 279-290.

Jouzel, J., Vaikmae, R., Petit, J. R., Martin, M., Duclos, Y., Stievenard, M., Lorius, C., Toots, M., Mélières M.A., Burckle, L.H., Barkov, N. I., Kotlyakov, V.M. (1995). The two-step shape and timing of the last deglaciation in Antarctica. Climate Dynamics, 11(3), 151-161.

Jouzel, J., Masson-Delmotte, V., Cattani, O., Dreyfus, G., Falourd, S., Hoffmann, G.,Minster, B., Nouet, J., Barnola, J.M., Chappellaz, J., Fischer, H., Gallet, J.C.,Johnsen, S., Leuenberger, M., Loulergue, L., Luethi, D., Oerter, H., Parrenin, F.,Raisbeck, G., Raynaud, D., Schilt, A., Schwander, J., Selmo, E., Souchez, R.,Spahni, R., Stauffer, B., Steffensen, J.P., Stenni, B., Stocker, T.F., Tison, J.L.,Werner, M., Wolff, E.W., 2007. Orbital and millennial Antarctic climate variability over the past 800,000 years. Science 317, 793–797.

Kaiser, J., & Lamy, F. (2010). Links between Patagonian Ice Sheet fluctuations and Antarctic dust variability during the last glacial period (MIS 4-2). Quaternary Science Reviews, 29(11), 1464-1471.

Kaplan, M. R., Moreno, P. I. and Rojas, M. (2008). Glacial dynamics in southernmost South America during Marine Isotope Stage 5e to the Younger Dryas chron: a brief review with a focus on cosmogenic nuclide measurements. J. Quaternary Sci., Vol. 23 pp. 649–658. ISSN 0267-8179.

Kaplan, M.R., Hein, A.S., Hubbard, A., Lax, S.M. Can glacial erosion limit the extent of glaciation? (2009) Geomorphology, 103 (2), pp. 172-179.

Kawamura, K., and the Dome Fuji Ice Core Project Members (2017). State dependence of climatic instability over the past 720,000 years from Antarctic ice cores and climate modeling. Science advances, 3(2), e1600446.

Krinner, G., & Genthon, C. (2003). Tropospheric transport of continental tracers towards Antarctica under varying climatic conditions. Tellus B, 55(1), 54-70.

Krinner, G., Petit, J. R., & Delmonte, B. (2010). Altitude of atmospheric tracer transport towards Antarctica inpresent and glacial climate. Quaternary science reviews, 29(1), 274-284.

Lambert, F., Delmonte, B., Petit, J. R., Bigler, M., Kaufmann, P. R., Hutterli, M. A., Stocker, T.F., Ruth, U., Steffensen, J.P., Maggi, V. (2008). Dust-climate couplings over the past 800,000 years from the EPICA Dome C ice core. Nature, 452(7187), 616-619.

Legrand, M., & Mayewski, P. (1997). Glaciochemistry of polar ice cores: a review. Reviews of Geophysics, 35(3), 219-243.

Li, F., Ginoux, P., & Ramaswamy, V. (2008). Distribution, transport, and deposition of mineral dust in the Southern Ocean and Antarctica: Contribution of major sources. Journal of Geophysical Research: Atmospheres, 113(D10).

Lorius, C., Merlivat, L., Jouzel, J., & Pourchet, M. (1979). A 30,000-yr isotope climatic record from Antarctic ice. Nature, 280, 644-648.

Mahowald, N., Kohfeld, K., Hansson, M., Balkanski, Y., Harrison, S. P., Prentice, I. C., Schulz, M., Rodhe, H. (1999). Dust sources and deposition during the last glacial maximum and current climate: A comparison of model results with paleodata from ice cores and marine sediments. Journal of Geophysical Research: Atmospheres, 104(D13), 15895-15916.

McArthur, J. M. (2010). Strontium isotope stratigraphy. Application of modern stratigraphic techniques: theory and case histories, edited by: Ratcliffe, KT and Zaitlin, BA, SEPM Spec. P, 94, 129-142.

Moreno, P. I., Lowell, T. V., Jacobson Jr, G. L., & Denton, G. H. (1999). Abrupt Vegetation and Climate Changes During the Last Glacial Maximum and Last Termination in The Chilean Lake District: A Case Study from Canal De La Puntilla (41° S). Geografiska Annaler: Series A, Physical Geography, 81(2), 285-311.

Narcisi, B., Petit, J. R., Delmonte, B., Scarchilli, C., & Stenni, B. (2012). A 16,000-yr tephra framework for the Antarctic ice sheet: a contribution from the new Talos Dome core. Quaternary Science Reviews, 49, 52-63.

Parish, T. R., & Bromwich, D. H. (1991). Continental-scale simulation of the Antarctic katabatic wind regime. Journal of Climate, 4(2), 135-146.

Petit, J.R., Jouzel, J., Raynaud, D., Barkov, N.I., Barnola, J.M., Basile, I., Bender, M., Chappellaz, J., Davis, M., Delaygue, G., Delmotte, M., Kotlyakov, V.M.,Legrand, M., Lipenkov, V.Y., Lorius, C., Pe´ pin, L., Ritz, C., Saltzman, E., Stievenard, M., 1999. Climate and atmospheric history of the past 420,000 years from the Vostok ice core, Antarctica. Nature 399, 429–436.

Petit, J. R., & Delmonte, B. (2009). A model for large glacial–interglacial climate-induced changes in dust and sea salt concentrations in deep ice cores (central Antarctica): Palaeoclimatic implications and prospects for refining ice core chronologies. Tellus B, 61(5), 768-790.

Prospero, J. M., Ginoux, P., Torres, O., Nicholson, S. E., & Gill, T. E. (2002). Environmental characterization of global sources of atmospheric soil dust identified with the Nimbus 7 Total Ozone Mapping Spectrometer (TOMS) absorbing aerosol product. Reviews of geophysics, 40(1).

Ram, M., Gayley, R. I., & Petit, J. R. (1988). Insoluble particles in Antarctic ice: background aerosol size distribution and diatom concentration. Journal of Geophysical Research: Atmospheres, 93(D7), 8378-8382.

Revel-Rolland, M., De Deckker, P., Delmonte, B., Hesse, P. P., Magee, J. W., Basile-Doelsch, I., Grousset, F., Bosch, D. (2006). Eastern Australia: a possible source of dust in East Antarctica interglacial ice. Earth and Planetary Science Letters, 249(1), 1-13.

Scherer, R. P., DeConto, R. M., Pollard, D., & Alley, R. B. (2016). Windblown Pliocene diatoms and East Antarctic Ice Sheet retreat. Nature Communications, 7, 12957.

Spratt, R. M., & Lisiecki, L. E. (2016). A Late Pleistocene sea level stack. Climate of the Past, 12(4), 1079.

Sugden, D. E., McCulloch, R. D., Bory, A. J. M., & Hein, A. S. (2009). Influence of Patagonian glaciers on Antarctic dust deposition during the last glacial period. Nature Geoscience, 2(4), 281-285.

Vallelonga, P., Gabrielli, P., Balliana, E., Wegner, A., Delmonte, B., Turetta, C., Burton, G., Vanhaecke, F., Rosman, K.J.R., Hongh, S., Boutron, C.F., Cescon, P., Barbante, C. (2010). Lead isotopic compositions in the EPICA Dome C ice core and Southern Hemisphere Potential Source Areas. Quaternary Science Reviews, 29(1), 247-255.

Van de Vijver, B., Zidarova, R., Sterken, M., Verleyen, E., de Haan, M., Vyverman, W., Hinz, F., Sabbe, K. (2011). Revision of the genus Navicula ss (Bacillariophyceae) in inland waters of the Sub-Antarctic and Antarctic with the description of five new species. Phycologia, 50(3), 281-297.

Van de Vijver, B., Tavernier, I., Kellogg, T. B., Gibson, J., Verleyen, E., Vyverman, W., & Sabbe, K. (2012). Revision of type materials of antarctic diatom species (Bacillariophyta) described by West & West (1911), with the description of two new species. Fottea, (2).

Van de Vijver, B., Wetzel, C., Kopalová, K., Zidarova, R., & Ector, L. (2013). Analysis of the type material of Achnanthidium lanceolatum Brébisson ex Kützing (Bacillariophyta) with the description of two new Planothidium species from the Antarctic Region. Fottea, 13(2), 105-117.

Van de Vijver, B., Kopalová, K., Zidarova, R., & Levkov, Z. (2014). Revision of the genus Halamphora (Bacillariophyta) in the Antarctic Region. Plant Ecology and Evolution, 147(3), 374-391.

Veres, D., Bazin, L., Landais, A., Toyé Mahamadou Kele, H., Lemieux-Dudon, B., Parrenin, F., Martinerie, P., Blayo, E., Blunier, T., Capron, E., Chappellaz, J., Rasmussen. S. O., Severi, M., Svensson, A., Vinther, B., Wolff, E. (2013). The Antarctic ice core chronology (AICC2012): an optimized multi-parameter and multi-site dating approach for the last 120 thousand years. Climate of the Past, 9(4), 1733-1748.

Villanueva, U., Raposo, J. C., Castro, K., de Diego, A., Arana, G. & Madariaga, J. M. 2008. Raman spectroscopy speciation of natural and anthropogenic solid phases in river and estuarine sediments with appreciable amount of clay and organic matter. Journal of Raman Spectroscopy, 39, 1195–1203.

Wegner, A., Fischer, H., Delmonte, B., Petit, J. R., Erhardt, T., Ruth, U., Svensson, A., Vinther, B., Miller, H. (2015). The role of seasonality of mineral dust concentration and size on glacial/interglacial dust changes in the EPICA Dronning Maud Land ice core. Journal of Geophysical Research: Atmospheres, 120(19), 9916-9931.

Werner, M., Tegen, I., Harrison, S. P., Kohfeld, K. E., Prentice, I. C., Balkanski, Y., Rodhe, H., Roelandt, C. (2002). Seasonal and interannual variability of the mineral dust cycle under present and glacial climate conditions. Journal of Geophysical Research: Atmospheres, 107(D24).

Wolff, E. W., Fischer, H., Fundel, F., Ruth, U., Twarloh, B., Littot, G. C., Mulvaney, R., Röthlisberger, R., de Angelis, M., Boutron, C. F., Hansson, M., Jonsell, U., Hutterli, M. A., Lambert, F., Kaufmann, P., Stauffer, B., Stocker, T., Steffensen, J.P., Bigler, M., Siggaard-Andersen, M.L., Udisti, R., Becagli, S., Castellano, E., Severi, M., Wagenbach, D., Barbante, C., Gabrielli, P., Gaspari, V., Hansson, M. (2006). Southern Ocean sea-ice extent, productivity and iron flux over the past eight glacial cycles. Nature, 440(7083), 491-496.

Yung, Y. L., Lee, T., Wang, C. H., & Shieh, Y. T. (1996). Dust: A diagnostic of the hydrologic cycle during the Last Glacial Maximum. Science, 271(5251), 962.

Zidarova, R., Van De Vijver, B., Mataloni, G., Kopalová, K., & Nedbalová, L. (2009). Four new freshwater diatom species (Bacillariophyceae) from Antarctica. Cryptogamie Algologie, 30(4), 295.

FIGURE CAPTIONS

FIGURE 1

Map of Antarctica and South America during the Last Glacial Maximum.

Light grey areas represent present-day ice shelves, white areas represent present-day grounded ice (from Fretwell et al., 2013). The grounding line around Antarctica at 20 ka is marked in cyan (from Bentley et al., 2014) (thick).Cyan area represents glacial coverage on South America during LGM (ca 28-16 ka) (Kaplan et al., 2008; 2009). Yellow line is -120 m contour line for South America and Subantarctic (extracted and simplified from Amante and Eakins, 2009).

FIGURE 2

Dust and climate records from Dome B on AICC2012 chronology (Veres et al., 2013). (A) Stable isotope record from Jouzel et al. (1995), proxy for paleotemperature, and global sea level curve from Spratt & Lisiecki (2016). (B) Dust profile from the Dome B ice core (light grey line, Delmonte et al., 2004a) adjusted on AICC2012, and new data from this work (black open circles) with mean value (grey circle) and standard deviation for each ice core bag. (C) Fine Particle Percent (FPP) variability along the core; light grey open circles represent data from Delmonte et al. (2004a), black open circles, with mean value and standard deviation, represent data from this work.

FIGURE 3

Volume (mass) dust size distributions at Dome B. (A) and (B) represent fine mode and coarse mode dust events, respectively. Raw dust size distributions are fitted with a 4-parameters Weibull function and dust mode indicated by the arrows. (C) Dust concentration versus size at Dome B; open circles represent data from Delmonte et al. (2004a), grey circles data from this work.

FIGURE 4

Sr and Nd isotopic composition ($\varepsilon_{Nd}(0)$ *vs* $^{87}Sr/^{86}Sr$) of central East Antarctic dust from MIS2 and early deglaciation. The age of Dome B and *old* Dome C samples is reported in table 1. The triangles represent data from Dome B and the size of the symbols is proportional to the modal value of dust within the sample. Red crosses represent EPICA Dome C data from MIS2, dark yellow crosses data from Komsomolskaia, dark green crosses data from the *old* Dome C ice core.

Data references: Basile et al. (1997), Delmonte et al. (2004a, 2004b, and this work). The green star represents the very first *old* Dome C ice core sample (Grousset et al., 1992), probably containing cryptotephra (see text). On the top right side of the figure we report ±2 std.dev of the Sr and Nd standards (2 ng).

FIGURE 5A

Strontium and Neodymium isotopic composition of central East Antarctic dust (MIS2) compared to fine-grained samples from the most important southern Hemisphere dust sources, South America and Eastern Australia. References for ice core data are the same as in figure 4. South American data are from Basile et al. (1997), Gaiero et al. (2003), Delmonte et al. (2004b), Gaiero et al. (2007), Gaiero (2007), Sugden et al. (2009), Gili et al. (in review). Australian data are from Revel-Rolland et al. (2016) and Gingele & DeDeckker (2005). CWA: Central Western Argentina, as defined by Gili et al. (2016).

FIGURE 5B

Strontium and Neodymium isotopic composition of central East Antarctic dust (MIS2) compared to bulk and fine sediment samples from South America. Data references are the same as in figure 4 and 5A; the yellow band shows the $\varepsilon_{Nd}(0)$ interval for Argentine Continental Shelf (ACS) reported by De Mahiques et al. (2008).

FIGURE 6

Pie charts showing the proportion of terrigenous (green), volcanic (dark yellow), authigenic/unknown (dark cyan) and marine (orange) minerals for each Dome B ice core sample analyzed by single-grain Raman mineralogy. Percentages are expressed in terms of number of counts. For each sample, the list of mineral species identified, along with their abundance, is reported in Table 2. The name of each sample is a number referring to the bottom depth of each bag. Next to each sample name, we report the approximate age expressed on AICC2012 chronology.

FIGURE 7A

Scanning Electron Microscope images of benthic/epiphytic diatoms found in the Dome B ice core. Top images (left and right): *Diploneis sp*, internal valve views. Bottom left: *Luticola* cf *cohnii* (Van de Vijver et al., 2011), internal valve view. Bottom right: *Amphora* sp. or *Halamphora* sp. (Van de Vijver et al., 2014), cingular view of the ariphid part.

FIGURE 7B

Scanning Electron Microscope images of freshwater Antarctic diatoms in the Dome B ice core.

Top left: *Placoneis australis* (Zidarova et al., 2009), external valve view. Top right: *Placoneis cf. australis,* external valve view. Middle left: *Planothidium* cf. *rostrolanceolatum* (Van de Vijver et al., 2013), external valve view. Middle right: *Navicula* cf. *Shackletoni* (Van de Vijver et al., 2012), external cingular view. Bottom left: *Navicula cremeri* (Van de Vijver et al., 2011). Bottom right: *Navicula* cf *australohetlandica* (Van de Vijver et al., 2011), internal valve view.

TABLE 1

Radiogenic isotope composition of Antarctic ice core dust samples.

Dome B and *old* Dome C ice core samples analyzed in this work are reported along with earlier Dome B data.

Column 1: $^{87}Sr/^{86}Sr$ isotopic composition of samples (± 2 std. dev.*10^{-6}). Errors are reported as 2 std. dev., ±0.000028, based on the repeated measurements of the NBS 987 (n=10), unless the internal error, 2 std. error, during the measurement is larger. In this case, the 2 std. error is reported. Columns 2 and 3: $^{143}Nd/^{144}Nd$ and $\varepsilon_{Nd}(0)$ isotopic composition of samples (±2 std error *10-6). Errors for the $^{143}Nd/^{144}Nd$ ratio are reported as 2 std. errors for each measurement because they are larger than the reproducibility of the 2 ng nNdβ standard of ±0.000038 2 std. dev., (n=10). Columns 4 and 5: dust concentration (ppb) and mode (µm) of volume size distribution of samples, from Coulter Counter measurements. Column 6: Age of sample (AICC2012 chronology, Veres et al., 2013).

TABLE 2

Single-grain Raman spectroscopy data.

Sample name, depth interval selected inside each bag, age, dust mode and concentration. Column 1: mineral species. Columns 2 to 9: number of grains and relative abundance (%) for each mineral species.

TABLE 1

Sample name	$^{87}Sr/^{86}Sr$	$^{143}Nd/^{144}Nd$	ε_{Nd} (0)	Dust conc. (ppb)	Mode (µm)	Age (kyr BP)	Reference
DB 520	0.708764 (29)*	0.512566 (22)	-1.40 (0.43)	349	2.39	16.5	This work
DB 540	0.708263 (28)*	0.512558 (16)	-1.56 (0.31)	441	2.17	17.5	This work
DB 580	0.708842 (28)*	0.512485 (38)	-2.98 (0.74)	1857	2.59	20.2	This work
DB 600	0.708747 (31)*	0.512491 (36)	-2.87 (0.70)	1384	2.71	21.7	This work
DB 620	0.709230 (28)*	0.512544 (42)	-1.83 (0.82)	578	2.10	23.3	This work
DB 631	0.708975 (33)*	0.512545 (26)	-1.81 (0.51)	840	2.43	24.0	This work
DB 640	0.708678 (28)*	0.512606 (27)	-0.62 (0.53)	2831	2.45	24.7	This work
DB 660	0.708533 (28)*	0.512545 (21)	-1.81 (0.41)	1261	2.46	26.2	This work
DB 700	0.709830 (28)*	0.512481 (34)	-3.06 (0.66)	448	2.19	28.4	This work
DB 581(I)	0.708383 (32)	0.512608 (18)	-0.59 (0.35)	903	2.68	20.4	Delmonte et al., 2004a
DB 581(II)	0.708479 (18)	0.512613 (28)	-0.49 (0.55)	903	2.68	20.4	Delmonte et al., 2004a
DB 641	0.708544 (28)	0.512526 (29)	-2.19 (0.57)	1081	2.42	24.8	Delmonte et al., 2004a
ODC 588	0.708879 (28)*	0.512542 (13)	-1.87 (0.25)	522	2.00	20.4	This work
ODC 614	0.709211 (34)*	n.m.	n.m.	653	1.98	22.0	This work
ODC 627	0.709192 (28)*	0.512502 (19)	-2.65 (0.37)	666	2.08	22.8	This work

(*) = normalized to a NBS987 $^{87}Sr/^{86}Sr$ ratio of 0.710245

TABLE 2

	DB600		DB620		DB631		DB640	
sample depth	(42-62 cm from top)		(24-49 cm from top)		(50-66 cm from top)		(75-91 cm from top)	
age (AICC2012)	21.7 kyr BP		23.2 kyr BP		24 kyr BP		24.7 kyr BP	
dust mode, concentration	2.67 µm, 1426 ppb		2 µm, 600 ppb		2.43 µm, 850 ppb		2.43 µm, 1150 ppb	
	n. of grains	%	n. of grains	%	n. of grains	%	n. of grains	%
Quartz	37	21	19	13	22	14	19	13
Albite	24	13	11	8	16	10	19	13
Ca-Plagioclase	17	9	10	7	25	15	16	11
K-Feldspar	7	4	6	4	3	2	7	5
Calcite	0	0	20	14	7	4	4	3
Anatase	8	4	7	5	6	4	7	5
Brookite	1	1	0	0	0	0	0	0
Rutile	2	1	4	3	4	2	4	3
Apatite	2	1	0	0	0	0	2	1
Monazite	0	0	0	0	0	0	1	1
Epidote	1	1	1	1	0	0	2	1
Prehnite	0	0	0	0	0	0	1	1
Actinolite	0	0	0	0	1	1	0	0
Muscovite	38	21	5	3	16	10	17	12
Chlorite	1	1	0	0	1	1	4	3
Dickite	0	0	0	0	0	0	1	1
Pyrophillite	0	0	0	0	1	1	0	0
Talc	0	0	4	3	1	1	1	1
Goethite	13	7	7	5	10	6	3	2
Hematite	1	1	7	5	4	2	1	1
Al-hydroxides	0	0	0	0	1	1	0	0
Total terrigenous	**152**	***84***	**101**	***70***	**118**	***73***	**109**	***75***
Sanidine	5	3	3	2	1	1	3	2
Ternary Feldspar	4	2	2	1	1	1	2	1
Zeolite	16	9	5	3	5	3	15	10
Augite	0	0	0	0	1	1	2	1
Total volcanic	**25**	***14***	**10**	***7***	**8**	***5***	**22**	***15***
Chalcedony	0	0	0	0	1	1	0	0
Sulphate	0	0	0	0	1	1	2	1
Nitratine	0	0	4	3	0	0	0	0
Natrite	1	1	0	0	0	0	0	0
Total authigenic/unknown	**1**	*1*	**4**	*3*	**2**	*1*	**2**	*1*
Aragonite	2	1	28	19	34	21	12	8
Cristobalite	0	0	1	1	0	0	1	1
Total marine	**2**	***1***	**29**	***20***	**34**	***21***	**13**	***9***
Total particles	**180**		**144**		**162**		**146**	

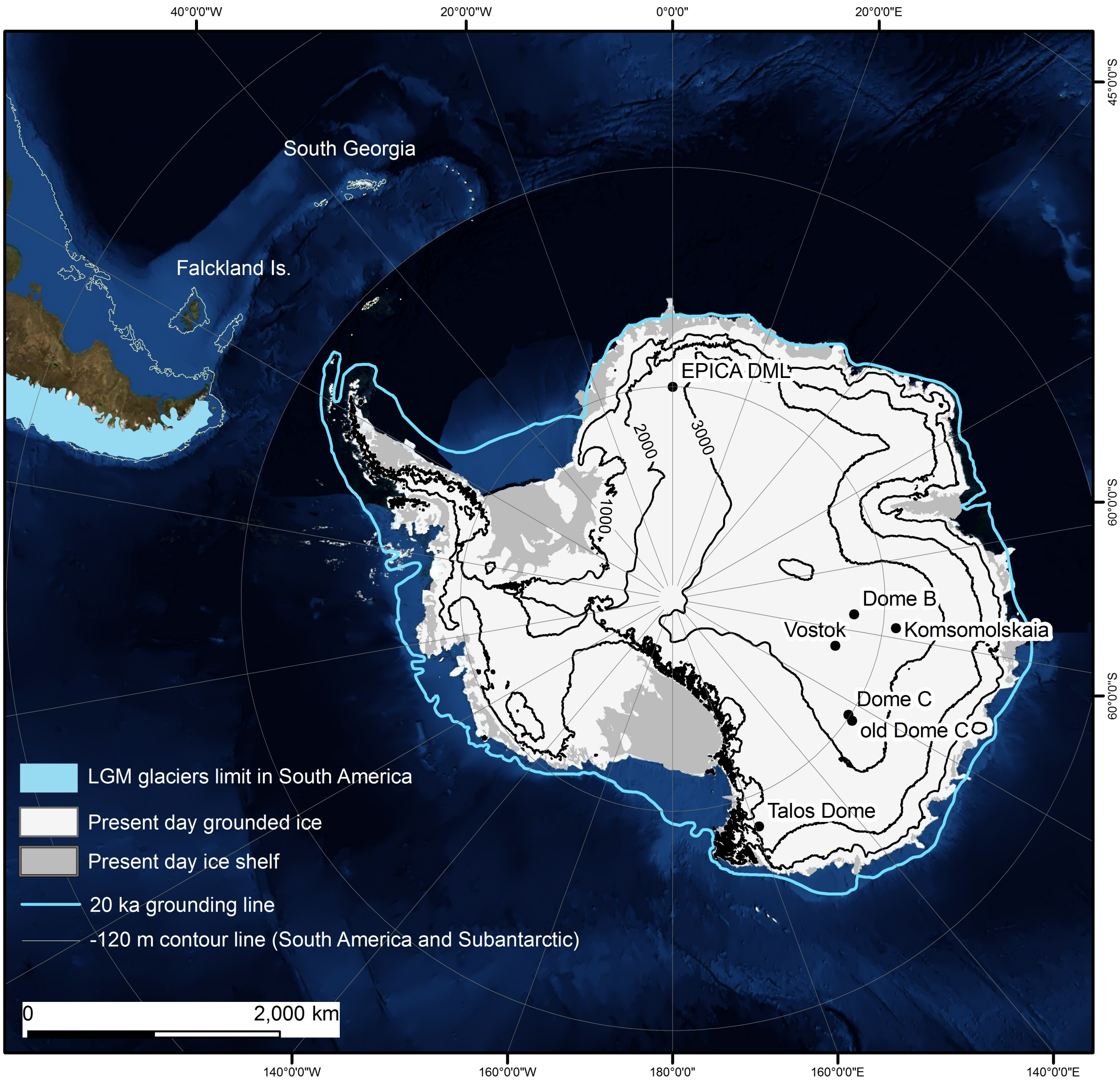
40°0'0"W
20°0'0"W
0°0'0"
20°0'0"E
45°0'0"S
60°0'0"S
60°0'0"S
140°0'0"W
160°0'0"W
180°0'0"
160°0'0"E
140°0'0"E
South Georgia
Falckland Is.
EPICA DML
3000
2000
1000
Dome B
Vostok
Komsomolskaia
Dome C
old Dome C
Talos Dome
LGM glaciers limit in South America
Present day grounded ice
Present day ice shelf
20 ka grounding line
-120 m contour line (South America and Subantarctic)
0
2,000 km

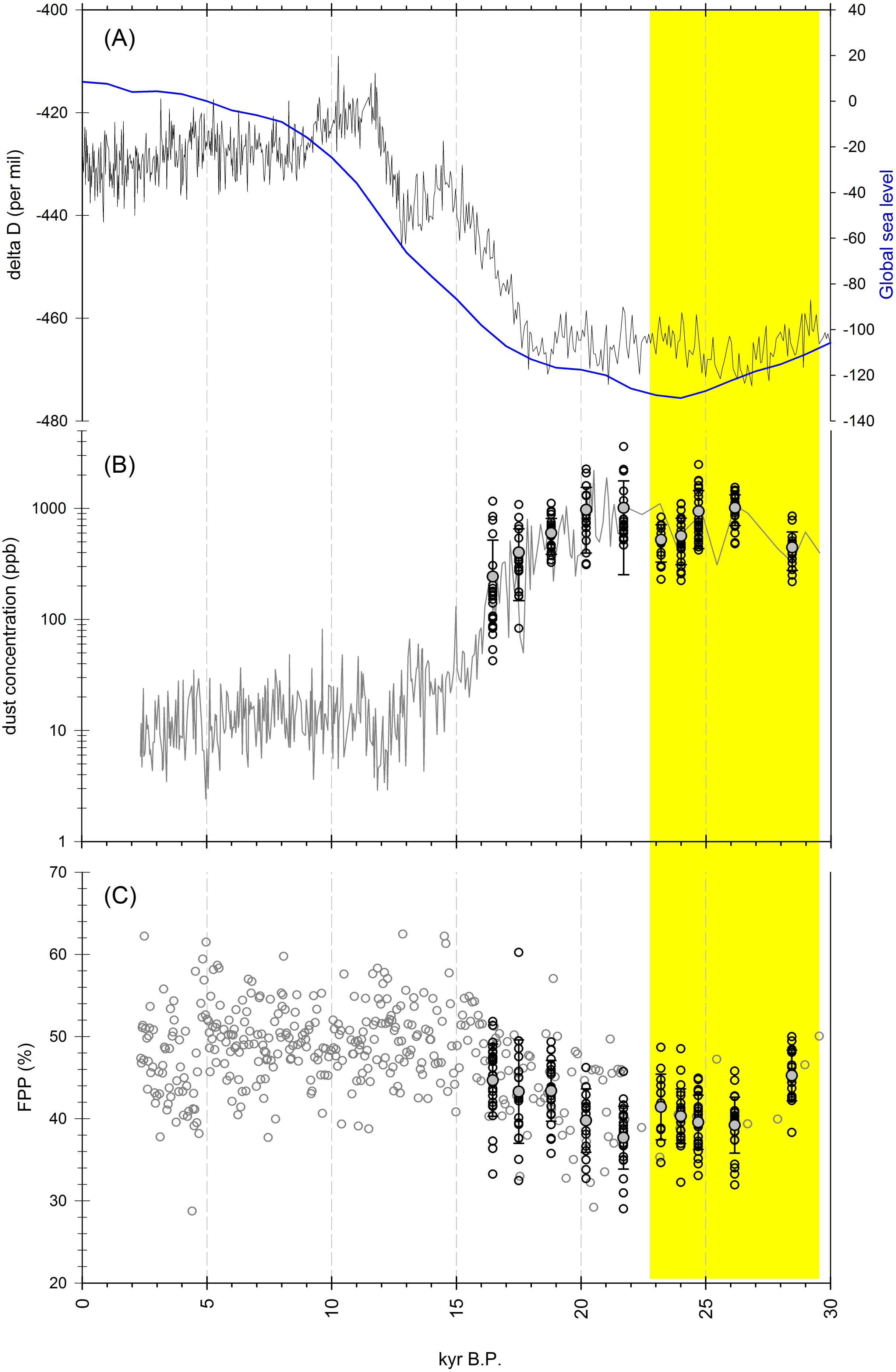

(A)
(B)
(C)
delta D (per mil)
Global sea level
dust concentration (ppb)
FPP (%)
kyr B.P.
-400
-420
-440
-460
-480
40
20
0
-20
-40
-60
-80
-100
-120
-140
1000
100
10
1
70
60
50
40
30
20
0
5
10
15
20
25
30

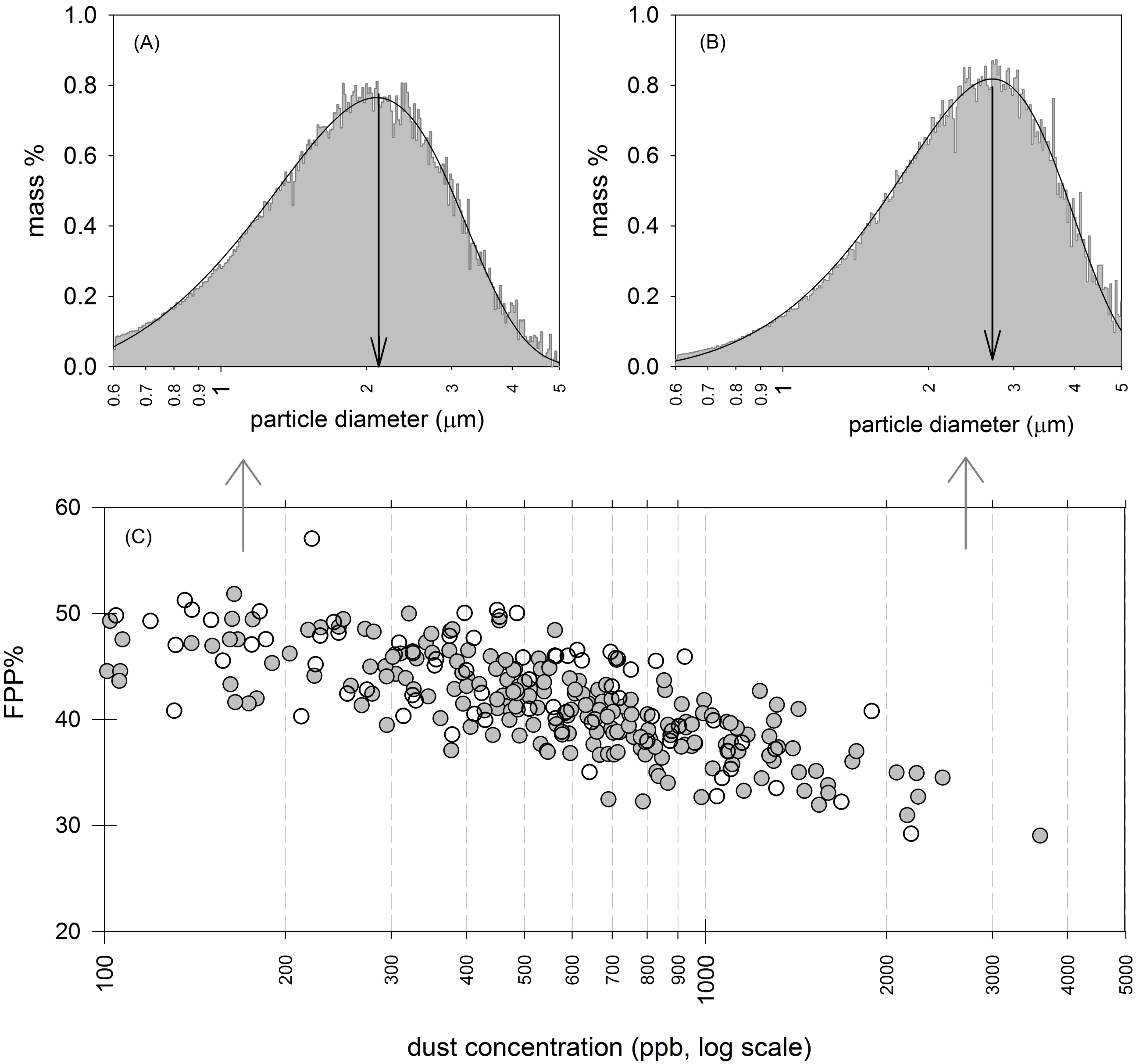

(A)
mass %
particle diameter (μm)
(B)
mass %
particle diameter (μm)
(C)
FPP%
dust concentration (ppb, log scale)

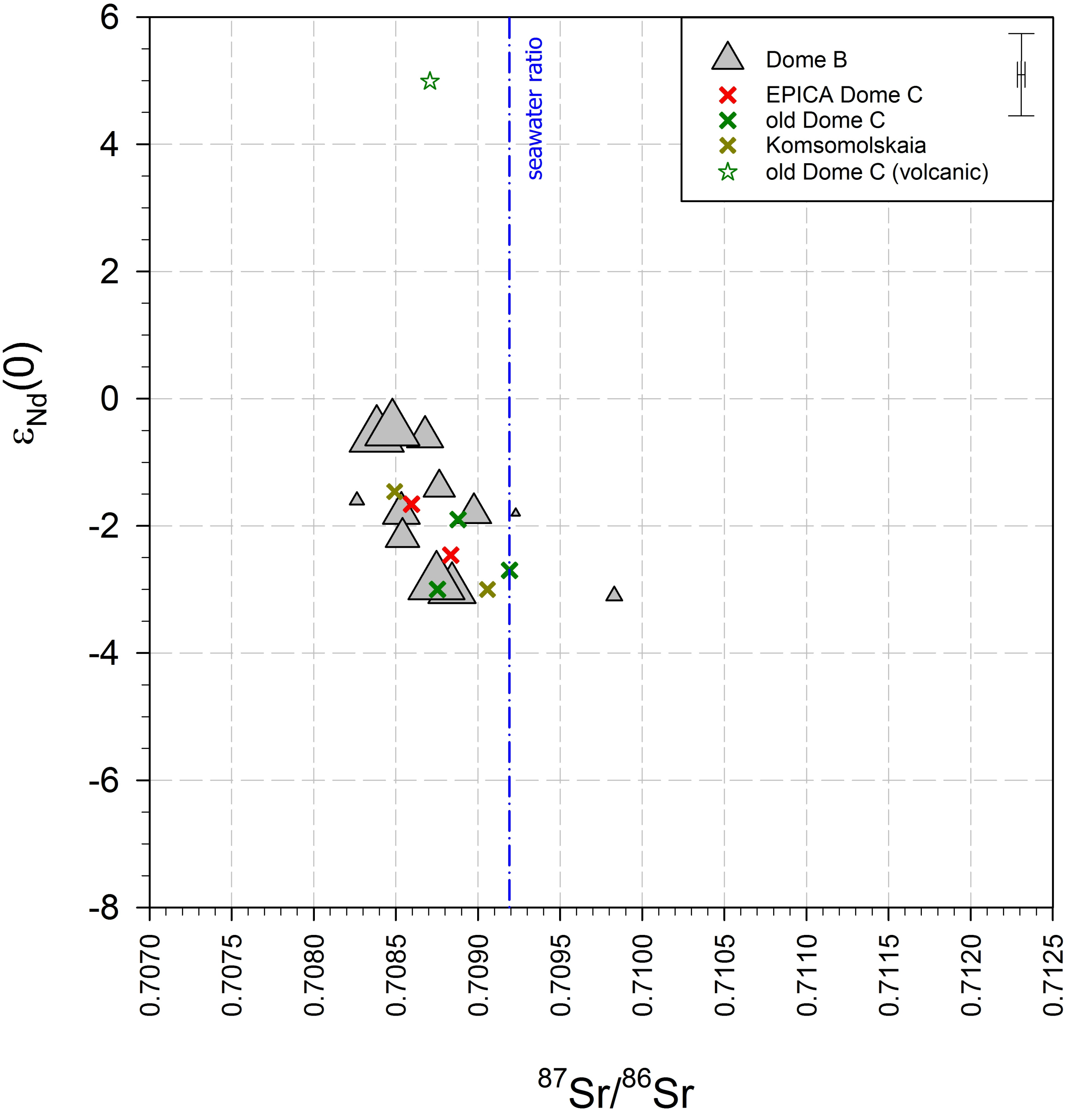

εNd(0)
87Sr/86Sr
seawater ratio
Dome B
EPICA Dome C
old Dome C
Komsomolskaia
old Dome C (volcanic)
6
4
2
0
-2
-4
-6
-8
0.7070
0.7075
0.7080
0.7085
0.7090
0.7095
0.7100
0.7105
0.7110
0.7115
0.7120
0.7125

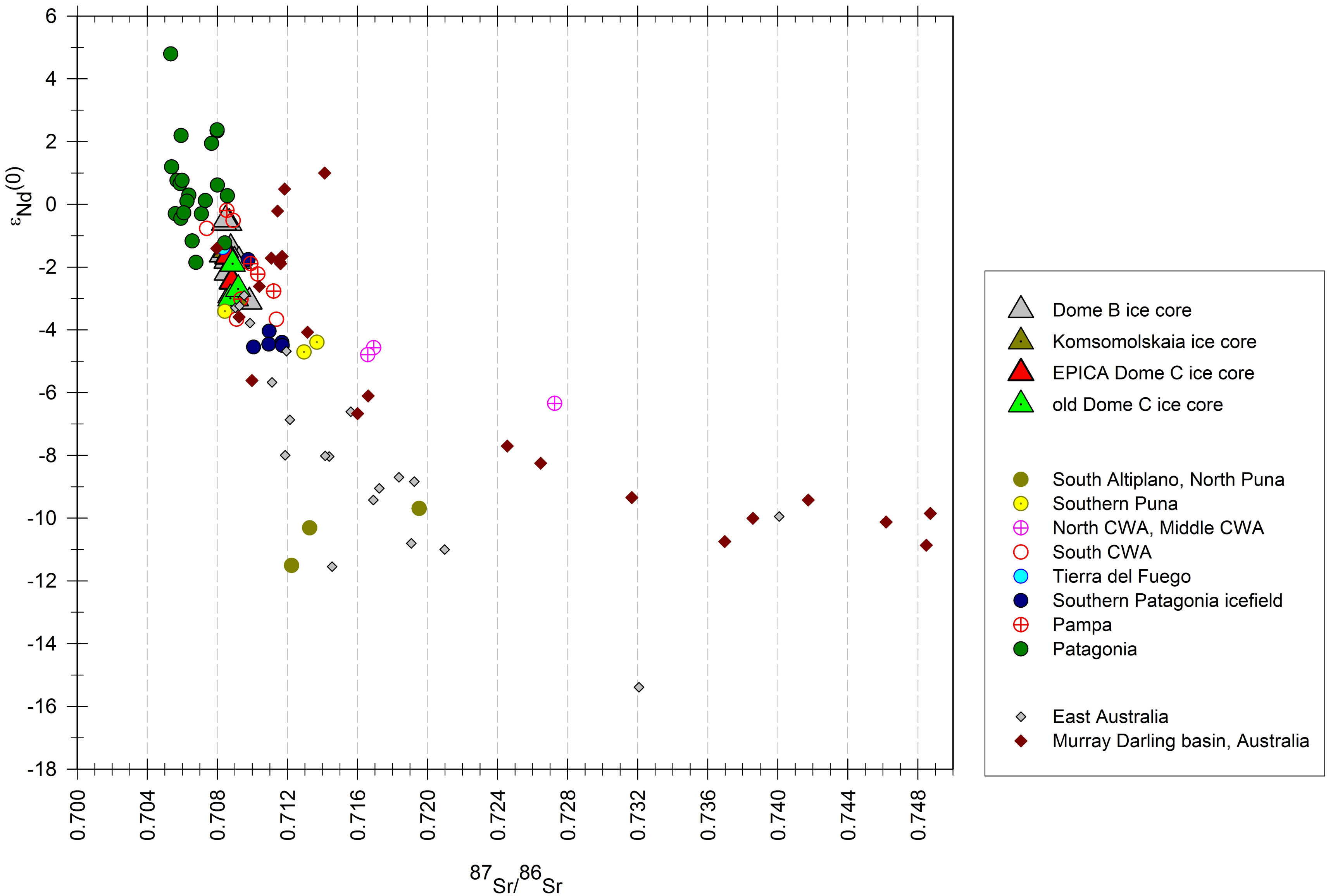

6
4
2
0
-2
-4
-6
-8
-10
-12
-14
-16
-18
$\varepsilon_{Nd}(0)$
0.700
0.704
0.708
0.712
0.716
0.720
0.724
0.728
0.732
0.736
0.740
0.744
0.748
$^{87}Sr/^{86}Sr$
Dome B ice core
Komsomolskaia ice core
EPICA Dome C ice core
old Dome C ice core
South Altiplano, North Puna
Southern Puna
North CWA, Middle CWA
South CWA
Tierra del Fuego
Southern Patagonia icefield
Pampa
Patagonia
East Australia
Murray Darling basin, Australia

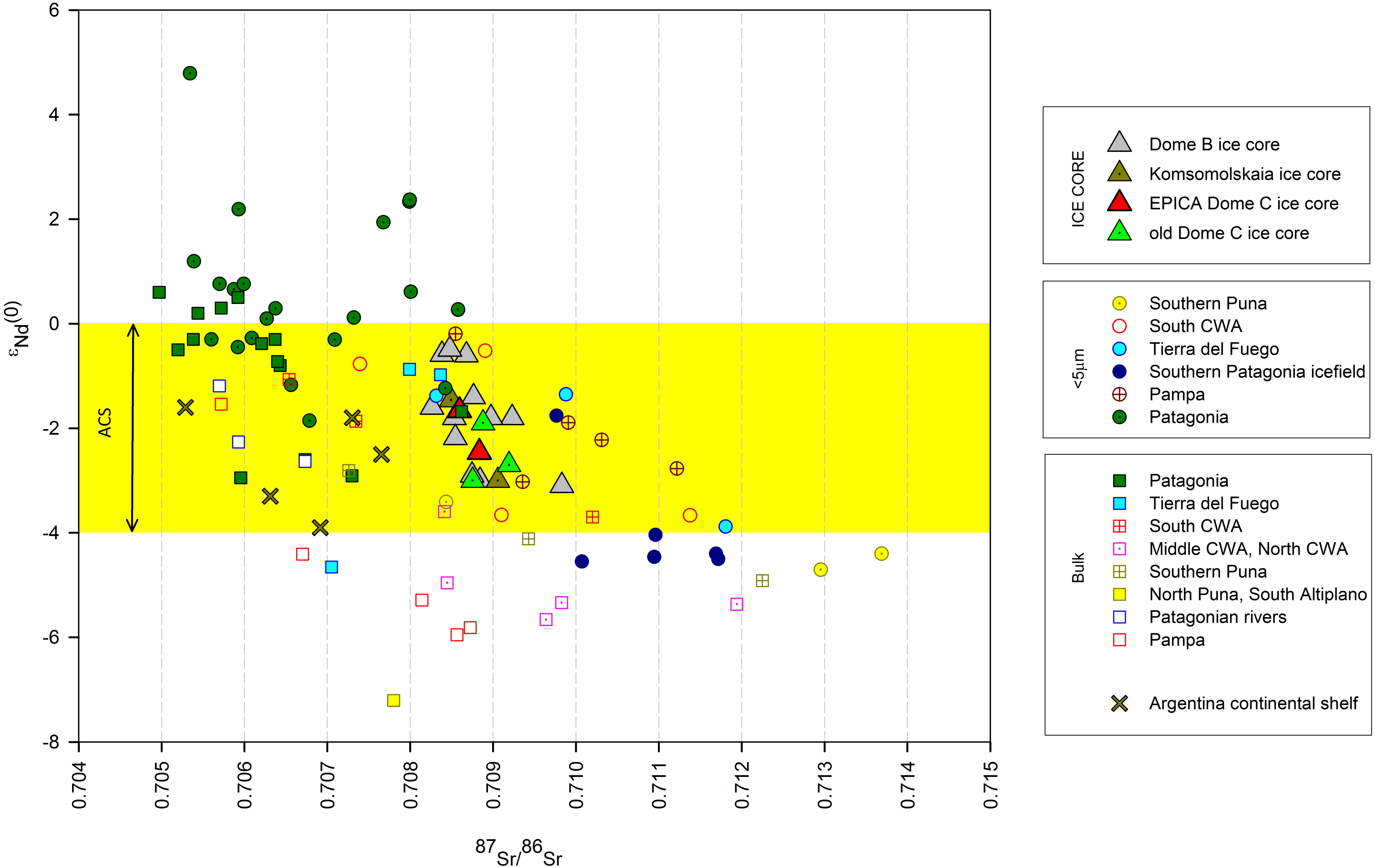

6
4
2
0
-2
-4
-6
-8
εNd(0)
ACS
0.704
0.705
0.706
0.707
0.708
0.709
0.710
0.711
0.712
0.713
0.714
0.715
87Sr/86Sr
ICE CORE
Dome B ice core
Komsomolskaia ice core
EPICA Dome C ice core
old Dome C ice core
<5µm
Southern Puna
South CWA
Tierra del Fuego
Southern Patagonia icefield
Pampa
Patagonia
Bulk
Patagonia
Tierra del Fuego
South CWA
Middle CWA, North CWA
Southern Puna
North Puna, South Altiplano
Patagonian rivers
Pampa
Argentina continental shelf

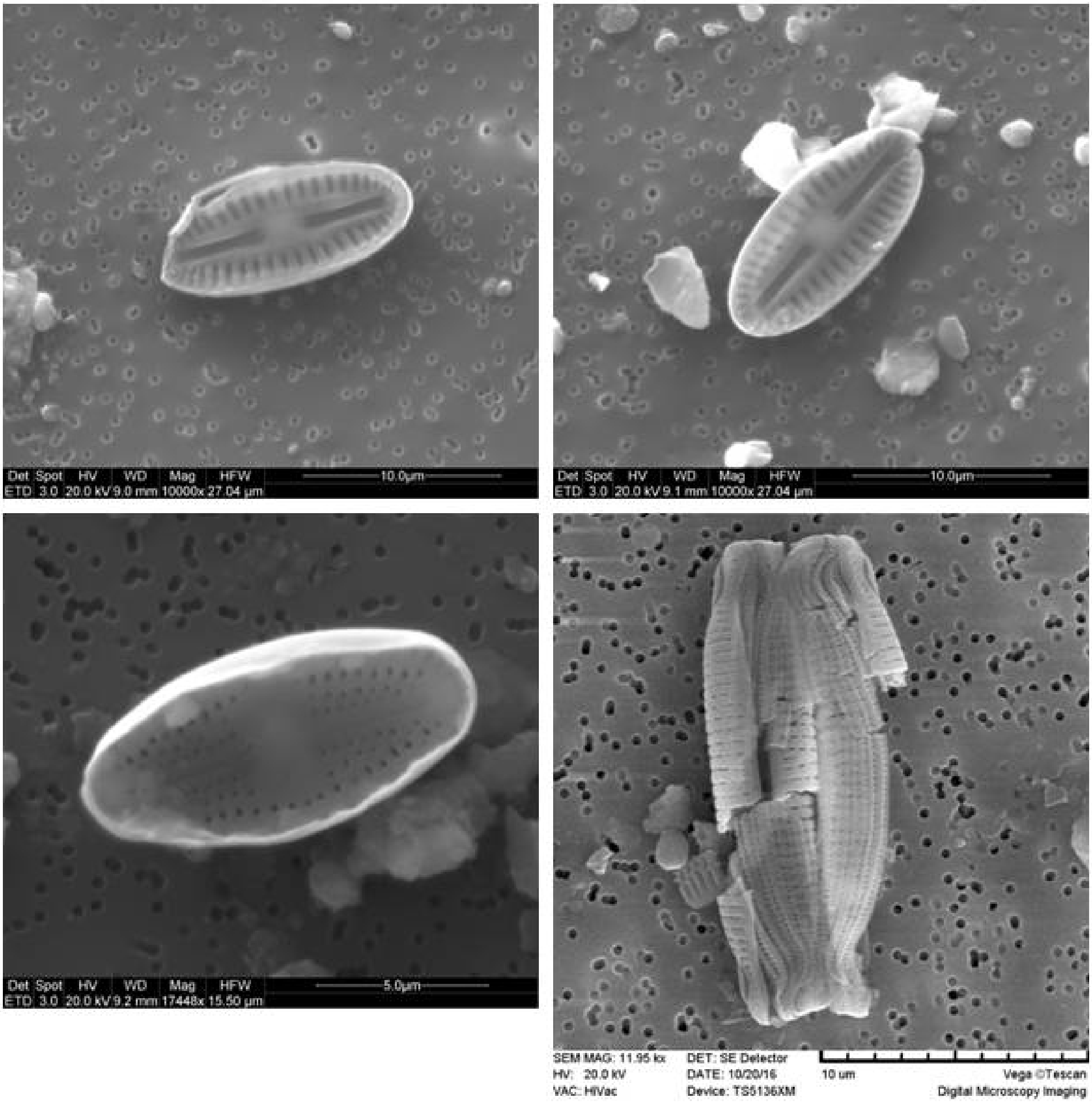
Det Spot HV WD Mag HFW
ETD 3.0 20.0 kV 9.0 mm 10000x 27.04 µm
10.0µm
Det Spot HV WD Mag HFW
ETD 3.0 20.0 kV 9.1 mm 10000x 27.04 µm
10.0µm
Det Spot HV WD Mag HFW
ETD 3.0 20.0 kV 9.2 mm 17448x 15.50 µm
5.0µm
SEM MAG: 11.95 kx
DET: SE Detector
HV: 20.0 kV
DATE: 10/20/16
VAC: HiVac
Device: TS5136XM
10 um
Vega ©Tescan
Digital Microscopy Imaging

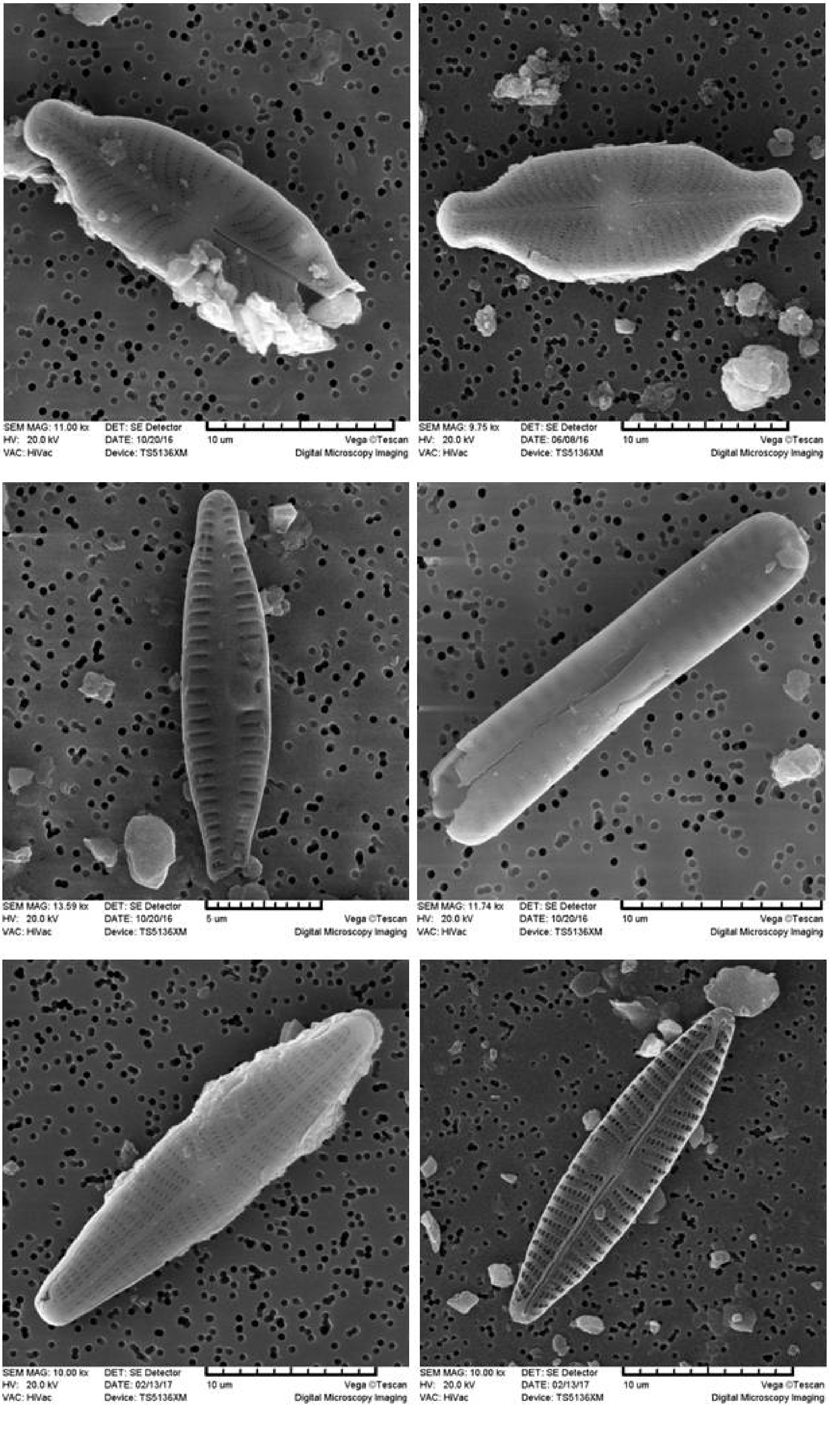
SEM MAG: 11.00 kx
DET: SE Detector
HV: 20.0 kV
DATE: 10/20/16
VAC: HiVac
Device: TS5136XM
10 um
Vega ©Tescan
Digital Microscopy Imaging
SEM MAG: 9.75 kx
DET: SE Detector
HV: 20.0 kV
DATE: 06/08/16
VAC: HiVac
Device: TS5136XM
10 um
Vega ©Tescan
Digital Microscopy Imaging
SEM MAG: 13.59 kx
DET: SE Detector
HV: 20.0 kV
DATE: 10/20/16
VAC: HiVac
Device: TS5136XM
5 um
Vega ©Tescan
Digital Microscopy Imaging
SEM MAG: 11.74 kx
DET: SE Detector
HV: 20.0 kV
DATE: 10/20/16
VAC: HiVac
Device: TS5136XM
10 um
Vega ©Tescan
Digital Microscopy Imaging
SEM MAG: 10.00 kx
DET: SE Detector
HV: 20.0 kV
DATE: 02/13/17
VAC: HiVac
Device: TS5136XM
10 um
Vega ©Tescan
Digital Microscopy Imaging
SEM MAG: 10.00 kx
DET: SE Detector
HV: 20.0 kV
DATE: 02/13/17
VAC: HiVac
Device: TS5136XM
10 um
Vega ©Tescan
Digital Microscopy Imaging